

# Thermodynamics of the Self-Assembly of *N*-Annulated Perylene Bisimides in Water. Disentangling the Enthalpic and Entropic Contributions

Manuel A. Martínez,<sup>‡a</sup> Daniel Aranda,<sup>‡b</sup> Enrique Ortí,<sup>b</sup> Juan Aragón,<sup>\*b</sup> and Luis Sánchez<sup>\*a</sup>

## Table of Contents

<i>1.- Material and Methods</i>	S-2
<i>2.- Synthesis and Characterization</i>	S-3
<i>3.- Collection of spectra</i>	S-7
<i>4.- Supplementary Figures and Tables</i>	S-16
<i>Synthetic scheme</i>	S-16
<i>Concentration dependent <sup>1</sup>H NMR experiments</i>	S-17
<i>Thermodynamic parameters associated to the self-assembly of 1 in water</i>	S-18
<i>Van't Hoff plots</i>	S-18
<i>UV-Vis experiments in H<sub>2</sub>O/dioxane mixtures and thermodynamic parameters for 2–4</i>	S-18
<i>Emission spectra</i>	S-20
<i>VT-UV-Vis of 1 and 2 and thermodynamic parameters in decalin</i>	S-20
<i>Molecular dynamics</i>	S-21
<i>5.- References</i>	S-27

## Experimental Procedures

### 1.- Materials and methods

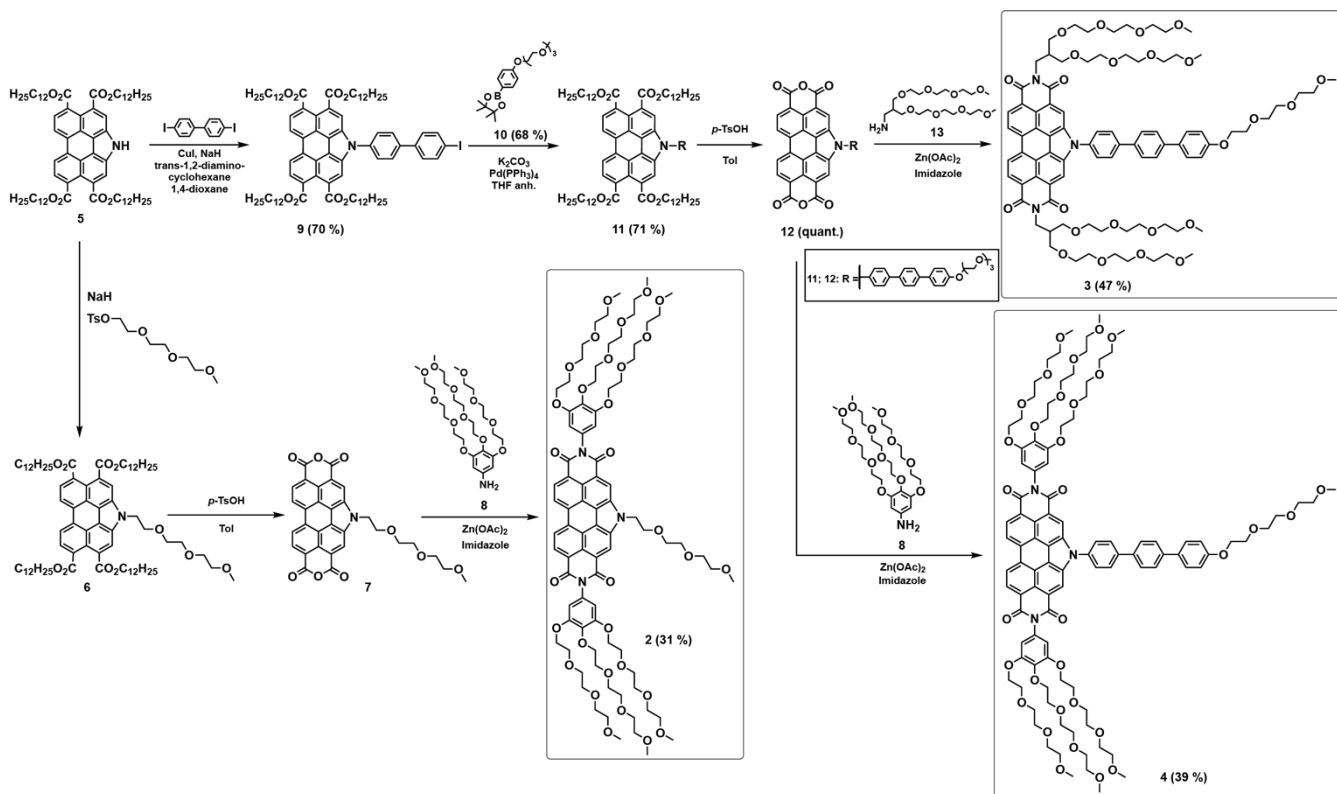
**General methods.** All solvents were dried according to standard procedures. Reagents were used as purchased. All air-sensitive reactions were carried out under argon atmosphere. Flash chromatography was performed using silica gel (Merck, Kieselgel 60, 230–240 mesh or Scharlau 60, 230–240 mesh). Analytical thin layer chromatography (TLC) was performed using aluminium-coated Merck Kieselgel 60 F254 plates. NMR spectra were recorded on a Bruker Avance 300 MHz ( $^1\text{H}$ : 300 MHz;  $^{13}\text{C}$ : 75 MHz) spectrometer at 298 K and a Bruker Avance 500 MHz ( $^1\text{H}$ : 500 MHz;  $^{13}\text{C}$ : 125 MHz) spectrometer at 323 K using partially deuterated solvents as internal standards. Coupling constants ( $J$ ) are denoted in Hz and chemical shifts ( $\delta$ ) in ppm. Multiplicities are denoted as follows: s = singlet, d = doublet, t = triplet, m = multiplet, br = broad. FT-IR spectra were recorded on a Bruker Tensor 27 (ATR device) spectrometer. UV-Vis spectra were registered on a Jasco-V630 spectrophotometer equipped with a Peltier thermoelectric temperature controller. The spectra were recorded in the continuous mode between 250 and 750 nm, with a wavelength increment of 1 nm, a response time of 4 s, and a bandwidth of 1 nm, by using a 1 cm quartz cuvette (Hellma). Thermal experiments were performed at constant heating rates of  $1\text{ }^\circ\text{C min}^{-1}$  from 10 to  $95\text{ }^\circ\text{C}$  in water. Emission spectra were registered on a Jasco FP-6300 spectrofluorometer. High resolution mass spectra (HRMS) were recorded on a MALDI Bruker daltonics Ultraflex TOF/TOF spectrometer.

**Computational details.** Molecular dynamics (MD) simulations in water as solvent were performed with GROMACS 2021.3 using periodic boundary conditions.<sup>S1</sup> For *N*-PBIs, we used the OPLS-AA force field with atom type selection as assigned by the PolyParGen tool<sup>S2</sup> for an initial structure with lateral chains totally extended and previously optimized at semiempirical level (GFN2-xTB).<sup>S3</sup> The initial structure for monomers, dimers and tetramers were centered in a box large enough so the minimum distance between the box boundary and the closest atom was of 1.0 nm to avoid spurious interactions due to the periodic boundary conditions. Point charges were calculated by following the RESP procedure with Antechamber at the B3LYP/6-31G\*\* level. For water molecules, we selected the widely-used TIP4P model.<sup>S1</sup> The standard protocol for MD simulations was followed: i) energy minimization, ii) solvent equilibration around the solute, and iii) production.

For energy minimization, we used a steepest descent algorithm with 0.01 nm step size until all forces were below  $1000\text{ kJ}\cdot\text{mol}^{-1}\cdot\text{nm}^{-1}$ . The equilibration of the solvent consisted of two stages of 0.1 ps in steps of 2 fs in which the solute was kept frozen: an initial NVT scheme fixing volume and temperature (300 K), and, subsequently, an NPT scheme where pressure (1 bar) and temperature (300 K) were kept constant. Finally, the production run (NPT scheme) consisted of 2 ns calculations in steps of 2 fs. In all cases, we used a V-rescale thermostat with damping constant of 0.1 ps and a Parrinello-Rahman pressure coupling with damping constant of 2 ps. C-H bonds in **1** and **3** and O-H bonds in water were constrained with a 4th order LINCS algorithm. The cutoff radius for short-range electrostatic and van der Waals interactions was set to 1.0 nm and we used an order 4 Particle Mesh Ewald for long-range electrostatics.

Thermodynamic properties were computed by averaging the values obtained for 2001 structures extracted from the production MD trajectory, one every each ps. For this step, we prepared a new set of calculations for dimers and tetramers keeping constant the concentration by fixing the PBI:H<sub>2</sub>O ratio to 1:3466 for **1** and 1:5406 for **3**. Aggregation enthalpies ( $\Delta\bar{H}_{agg}$ ) were estimated as the difference of the average enthalpy on the bonded state  $\bar{H}_b$  of  $n$  *N*-PBIs ( $n = 2$  for dimer and  $n = 4$  for tetramer) minus  $n$  times the average enthalpy of the non-bonded state  $\bar{H}_{nb}$  (monomer); namely,  $\Delta\bar{H}_{agg} = \bar{H}_b - n \cdot \bar{H}_{nb}$ . Changes in the intermolecular interactions between bonded and non-bonded structures were analyzed by decomposing the potential energy of the full system *N*-PBI/H<sub>2</sub>O ( $\bar{E}_{pot}$ ) into three average terms: potential energy of the *N*-PBIs compounds ( $\bar{E}_{pot}^{N-PBI}$ ), potential energy of the water molecules ( $\bar{E}_{pot}^{H_2O}$ ), and *N*-PBI/H<sub>2</sub>O interaction of the *N*-PBIs with water ( $\bar{E}_{int}^{N-PBI-H_2O}$ ). The two first terms were calculated by extracting separately the *N*-PBIs and the water molecules from the MD trajectory of the full system and re-computing the average potential energy for the corresponding subsystem, whereas  $\bar{E}_{int}^{N-PBI-H_2O}$  was computed as the difference between the two first terms and the average potential energy of the complete system  $\bar{E}_{pot}$ ; i.e.,  $\bar{E}_{int}^{N-PBI-H_2O} = \bar{E}_{pot} - \bar{E}_{pot}^{N-PBI} - \bar{E}_{pot}^{H_2O}$ .

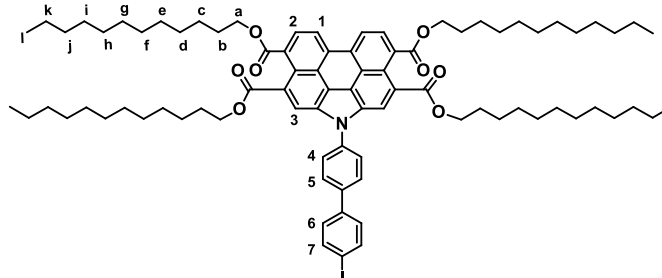
## 2.- Synthesis and Characterization



**Scheme S1.** Synthesis of amphiphilic *N*-PBIs **2–4**.

Compounds **1**,<sup>S5</sup> **5**,<sup>S6</sup> **6**,<sup>S5</sup> **7**,<sup>S5</sup> **8**,<sup>S7</sup> **10**,<sup>S8</sup> and **13**<sup>S9</sup> were prepared according to previously reported synthetic procedures and showed identical spectroscopic properties to those reported therein.

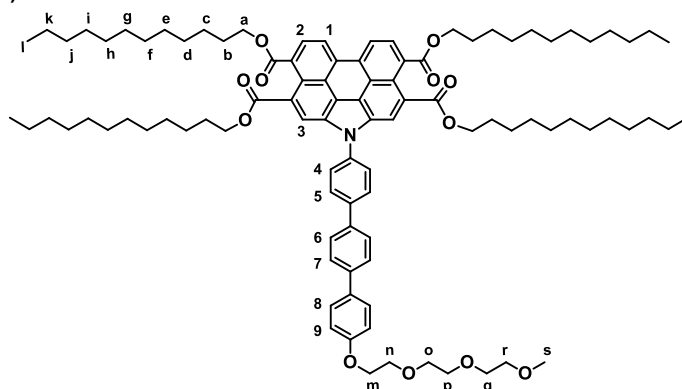
### Tetradecyl 1-(4'-iodo-[1,1'-biphenyl]-4-yl)-1*H*-phenanthro[1,10,9,8-*cdefg*]carbazole-3,4,9,10-tetracarboxylate (**9**)



$C_{84}H_{114}INO_8$   
Exact Mass: 1391.7589  
Mol. Wt.: 1392.7103

NaH (36 mg, 0.90 mmol) was slowly added to a mixture of compound **5** (200 mg, 0.18 mmol), 4,4'-diiodobiphenyl (405 mg, 0.90 mmol), copper iodide (17 mg, 0.09 mmol), and trans-1,2-diaminocyclohexane (105 mg, 0.90 mmol) in dry 1,4-dioxane (20 mL). The resulting mixture was refluxed overnight under argon atmosphere. After cooling to room temperature, the reaction mixture was poured into cold water and extracted with  $CH_2Cl_2$ . The resulting organic layer was dried over  $MgSO_4$ , filtered, and the solvent was evaporated under reduced pressure. The obtained product was purified by column chromatography (silica gel, Hex/ $CH_2Cl_2$  1/4) affording compound **9** as a yellow solid (175 mg, 70 %).  $^1H$  NMR ( $CDCl_3$ , 300 MHz)  $\delta$ /ppm 8.78 (2H,  $H_1$ , d,  $J = 8.0$  Hz), 8.57 (2H,  $H_3$ , s), 8.35 (2H,  $H_2$ , d,  $J = 7.9$  Hz), 8.02 – 7.80 (6H,  $H_{4+5+7}$ , m), 7.46 (2H,  $H_6$ , d,  $J = 8.4$  Hz), 4.44 – 4.33 (8H,  $H_a$ , m), 1.89 – 1.72 (8H,  $H_b$ , m), 1.50 – 1.16 (72H,  $H_{c-k}$ , m), 0.90 – 0.82 (12H,  $H_l$ , m).  $^{13}C$  NMR ( $CDCl_3$ , 75 MHz)  $\delta$ /ppm 169.4, 169.0, 139.6, 138.3, 137.7, 132.7, 132.0, 129.8, 129.5, 129.1, 129.0, 128.6, 125.4, 125.0, 124.4, 122.3, 119.7, 119.0, 93.9, 66.0, 65.9, 32.1, 29.8(3), 29.8(0), 29.7(7), 29.7(5), 29.7(1), 29.5, 28.8, 28.7, 26.2, 22.8, 14.3. FTIR (neat) 667, 727, 752, 799, 838, 874, 935, 1001, 1018, 1044, 1099, 1120, 1153, 1187, 1262, 1340, 1373, 1409, 1456, 1481, 1505, 1521, 1580, 1589, 1608, 1721, 2853, 2923, 2955  $cm^{-1}$ . HRMS (MALDI-TOF) calcd. for  $C_{84}H_{114}INO_8$   $[M]^+$ , 1391.759; found, 1391.636.

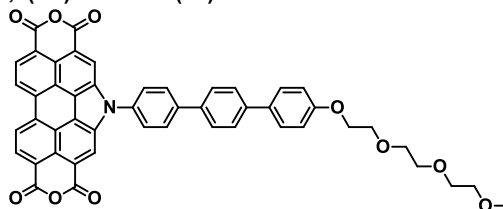
**Tetradodecyl 1-(4''-(2-(2-(2-methoxyethoxy)ethoxy)ethoxy)ethoxy)-[1,1':4',1''-terphenyl]-4-yl)-1*H*-phenanthro[1,10,9,8-*cdefg*]carbazole-3,4,9,10-tetracarboxylate (11)**



$C_{97}H_{133}NO_{12}$   
Exact Mass: 1503.9828  
Mol. Wt.: 1505.0934

Compound **9** (391 mg, 0.28 mmol), compound **10** (308 mg, 0.84 mmol), and tetrakis(triphenylphosphine)palladium(0) (71 mg, 0.06 mmol) were dissolved in dried THF (60 mL).  $K_2CO_3$  (194 mg, 1.40 mmol) was dissolved in water (1 mL) and added to the solution under argon atmosphere. The reaction mixture was heated to reflux overnight. After that, the solvent was evaporated under reduced pressure and the residue was then redissolved in  $CH_2Cl_2$  and washed with water. The organic layer was dried over  $MgSO_4$ , filtered, and the solvent was evaporated under reduced pressure. The obtained residue was purified by column chromatography (silica gel,  $CHCl_3/MeOH$  10/0.1) affording compound **11** as a light orange solid (302 mg, 71 %).  $^1H$  NMR ( $CDCl_3$ , 300 MHz)  $\delta$ /ppm 8.62 (2H,  $H_1$ , d,  $J = 8.0$  Hz), 8.54 (2H,  $H_3$ , s), 8.28 (2H,  $H_2$ , d,  $J = 8.0$  Hz), 7.99 (2H,  $H_5$ , d,  $J = 8.6$  Hz), 7.94 (2H,  $H_4$ , d,  $J = 8.6$  Hz), 7.79 (2H,  $H_6$ , d,  $J = 8.5$  Hz), 7.71 (2H,  $H_7$ , d,  $J = 8.5$  Hz), 7.60 (2H,  $H_8$ , d,  $J = 8.8$  Hz), 7.03 (2H,  $H_9$ , d,  $J = 8.8$  Hz), 4.39 (8H,  $H_a$ , m), 4.24 – 4.17 (2H,  $H_m$ , m), 3.94 – 3.88 (2H,  $H_n$ , m), 3.81 – 3.76 (2H,  $H_o$ , m), 3.75 – 3.70 (2H,  $H_p$ , m), 3.70 – 3.66 (2H,  $H_q$ , m), 3.61 – 3.55 (2H,  $H_r$ , m), 3.40 (3H,  $H_s$ , s), 1.91 – 1.72 (8H,  $H_b$ , m), 1.54 – 1.14 (72H,  $H_{c-k}$ , m), 0.92 – 0.78 (12H,  $H_i$ , m).  $^{13}C$  NMR (75 MHz,  $CDCl_3$ )  $\delta$ /ppm 169.3, 168.9, 158.7, 140.4, 140.1, 138.2, 137.2, 133.2, 132.4, 131.9, 129.5, 129.2, 128.8, 128.4, 128.1, 127.5, 127.3, 125.2, 124.8, 124.2, 122.0, 119.4, 119.1, 115.1, 72.1, 71.0, 70.8, 70.7, 69.9, 67.7, 65.9, 65.8, 59.2, 32.0, 29.8, 29.7(7), 29.7(5), 29.7(1), 29.5, 29.4, 28.8, 28.7, 26.2, 26.2, 22.8, 22.7, 14.2. FTIR (neat) 621, 670, 721, 751, 765, 800, 820, 839, 890, 952, 1003, 1015, 1047, 1153, 1187, 1209, 1258, 1317, 1351, 1378, 1423, 1467, 1492, 1534, 1590, 1608, 1668, 1715, 2853, 2922  $cm^{-1}$ . HRMS (MALDI-TOF) calcd. for  $C_{97}H_{133}NO_{12}$   $[M]^+$ , 1503.982; found, 1503.549.

**5-(4''-(2-(2-(2-methoxyethoxy)ethoxy)ethoxy)ethoxy)-[1,1':4',1''-terphenyl]-4-yl)-1*H*-pyrano[3',4',5':4,5]naphtha[2,1,8-*cde*]-pyrano-[3',4',5':4,5]naphtho[8,1,2-*gh*]isoindole-1,3,7,9(5*H*)-tetraone (12)**



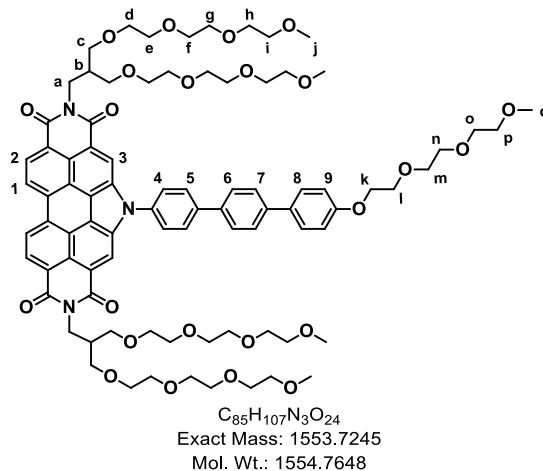
$C_{49}H_{33}NO_{10}$   
Exact Mass: 795.2104  
Mol. Wt.: 795.7870

A mixture of compound **11** (292 mg, 0.194 mmol) and *p*-toluene sulphonic acid monohydrate (185 mg, 0.97 mmol) in toluene (5 mL) was heated to reflux overnight. Still warm, MeOH was added to precipitate it. The mixture was filtered and washed with MeOH affording, without any further purification, compound **12** as a dark purple solid (154 mg, quant.). FTIR (neat) 685, 727, 744, 752, 798, 821, 903, 944, 999, 1023, 1041, 1066, 1121, 1175, 1209, 1267, 1325, 1385, 1413, 1458, 1494, 1539, 1561, 1601, 1752, 2854, 2924  $cm^{-1}$ . HRMS (MALDI-TOF) calcd. for  $C_{49}H_{33}NO_{10}$   $[M]^+$ , 795.210; found, 795.145.

### Synthesis of PBIs 2–4. General procedure.

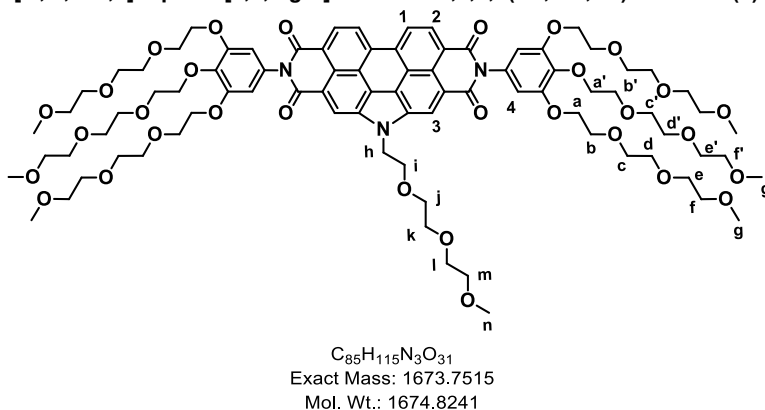
A mixture of compound **7** or **12** (0.063 mmol), amines **8** or **13** (0.148 mmol), zinc acetate (46 mg, 0.251 mmol) and imidazole (2.0 g) was heated to 110 °C overnight under argon atmosphere. After cooling at room temperature, the reaction mixture was extracted with CH<sub>2</sub>Cl<sub>2</sub> and washed with a saturated NaCl solution, the organic layer was dried over MgSO<sub>4</sub> and the solvent was evaporated under reduced pressure. After that, the residue obtained was purified by column chromatography.

### 2,8-bis(13-(2,5,8,11-tetraoxadodecyl)-2,5,8,11-tetraoxatetradecan-14-yl)-5-(4''-(2-(2-(2-methoxyethoxy)ethoxy)ethoxy)ethyl)-[1,1':4',1''-terphenyl]-4-yl)-1*H*-pyrido[3',4',5':4,5]naphtho[2,1,8-*cde*]pyrido[3',4',5':4,5]naphtho[8,1,2-*ghi*]isoindole-1,3,7,9-(2*H*,5*H*,8*H*)-tetraone (**2**)



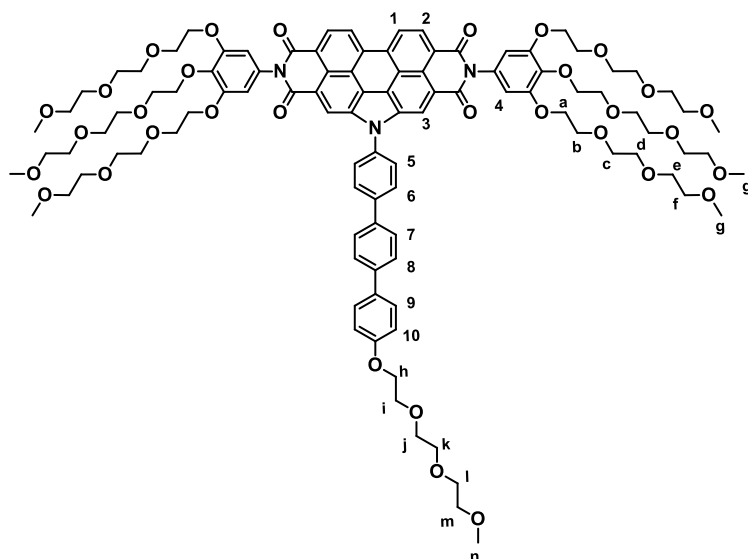
Compound **2** was obtained after column chromatography purification (silica gel, CHCl<sub>3</sub>/MeOH 10/0.1) as a viscous red solid (46 mg, 47 %). <sup>1</sup>H NMR (CDCl<sub>3</sub>, 300 MHz) δ/ppm 8.99 (2H, H<sub>3</sub>, s), 8.80 (2H, H<sub>1</sub>, d, *J* = 8.0 Hz), 8.71 (2H, H<sub>2</sub>, d, *J* = 8.0 Hz), 8.03 (2H, H<sub>5</sub>, d, *J* = 8.4 Hz), 7.97 (2H, H<sub>4</sub>, d, *J* = 8.4 Hz), 7.80 (2H, H<sub>6</sub>, d, *J* = 8.4 Hz), 7.73 (2H, H<sub>7</sub>, d, *J* = 8.4 Hz), 7.60 (2H, H<sub>8</sub>, d, *J* = 8.8 Hz), 7.03 (2H, H<sub>9</sub>, d, *J* = 8.8 Hz), 4.36 (4H, H<sub>a</sub>, d, *J* = 6.9 Hz), 4.25 – 4.19 (2H, H<sub>k</sub>, m), 3.95 – 3.89 (2H, H<sub>l</sub>, m), 3.82 – 3.77 (2H, m, m), 3.75 – 3.72 (2H, H<sub>n</sub>, m), 3.71 – 3.66 (2H, H<sub>o</sub>, m), 3.65 – 3.44 (62H, H<sub>p+(c-i)</sub>, m), 3.40 (3H, H<sub>q</sub>, s), 3.31 (12H, H<sub>j</sub>, s), 2.56 (2H, H<sub>b</sub>, m). <sup>13</sup>C NMR (CDCl<sub>3</sub>, 75 MHz) δ/ppm 165.0, 163.9, 158.7, 140.9, 140.6, 137.9, 136.7, 134.3, 133.1, 132.8, 129.2, 128.2, 127.6, 127.5, 125.0, 124.8, 124.1, 122., 121.8, 120.2, 119.9, 115.2, 72.1, 72.0, 71.0, 70.9, 70.8, 70.7, 70.6(4), 70.6(2), 70.5(4), 70.5(2), 69.9, 67.7, 59.2, 59.1. FTIR (neat) 624, 655, 666, 709, 741, 805, 821, 844, 877, 940, 1003, 1042, 1106, 1182, 1200, 1258, 1314, 1351, 1368, 1393, 1425, 1446, 1457, 1473, 1494, 1534, 1560, 1604, 1656, 1692, 2871 cm<sup>-1</sup>. HRMS (MALDI-TOF, exact mass) calcd. for C<sub>85</sub>H<sub>107</sub>N<sub>3</sub>O<sub>24</sub> [M+Na]<sup>+</sup>, 1576.7245; found, 1576.7217.

### 5-(2-(2-(2-methoxyethoxy)ethoxy)ethyl)-2,8-bis(3,4,5-tris(2-(2-(2-methoxyethoxy)ethoxy)ethoxy)phenyl)-1*H*-pyrido-[3',4',5':4,5]naphtho[2,1,8-*cde*]pyrido[3',4',5':4,5]naphtho[8,1,2-*ghi*]isoindole-1,3,7,9(2*H*, 5*H*,8*H*)-tetraone (**3**)



Compound **3** was obtained after column chromatography purification (silica gel, CHCl<sub>3</sub>/MeOH 10/0.3) as a viscous red solid (52 mg, 31 %). <sup>1</sup>H NMR (CDCl<sub>3</sub>, 500 MHz) δ/ppm 8.80 (2H, H<sub>3</sub>, s), 8.59 (2H, H<sub>1</sub>, d, *J* = 7.8 Hz), 8.44 (2H, H<sub>2</sub>, br), 6.79 (4H, H<sub>4</sub>, s), 4.97 (2H, H<sub>h</sub>, br), 4.28 (4H, H<sub>a'</sub>, t, *J* = 5.2 Hz), 4.13 (8H, H<sub>a</sub>, t, *J* = 5.0 Hz), 4.10 (2H, H<sub>i</sub>, br), 3.90 (4H, H<sub>b'</sub>, t, *J* = 5.2 Hz), 3.84 – 3.79 (12H, H<sub>b+c'</sub>, m), 3.74 – 3.69 (16H, H<sub>c+d'+e'</sub>, m), 3.67 – 3.62 (16H, H<sub>d+e</sub>, m), 3.62 – 3.58 (6H, H<sub>f+j</sub>, m), 3.56 – 3.54 (2H, H<sub>k</sub>, m), 3.54 – 3.51 (8H, H<sub>r</sub>, m), 3.44 – 3.42 (2H, H<sub>l</sub>, m), 3.41 (6H, H<sub>g'</sub>, s), 3.34 (12H, H<sub>g</sub>, s), 3.28 – 3.25 (2H, H<sub>m</sub>, m), 3.12 (3H, H<sub>n</sub>, s). <sup>13</sup>C NMR (CDCl<sub>3</sub>, 125 MHz) δ/ppm 164.7, 163.5, 153.0, 138.6, 134.8, 132.1, 131.2, 127.3, 124.0, 123.4, 122.1, 121.5, 120.9, 119.0, 118.8, 109.0, 72.5, 72.1, 72.0, 71.8, 71.1, 70.7, 70.6(8), 70.6(1), 70.5(5), 70.4(9), 70.4(1), 69.7, 69.1, 58.9, 58.8, 58.7. FTIR (neat) 635, 684, 710, 741, 769, 803, 849, 940, 1109, 1199 1243, 1303, 1352, 1377, 1399, 1425, 1504, 1558, 1600, 1662, 1697, 2874, 2923 cm<sup>-1</sup>. HRMS (MALDI-TOF, exact mass) calcd. for C<sub>85</sub>H<sub>115</sub>N<sub>3</sub>O<sub>31</sub> [M+Na]<sup>+</sup>, 1696.7412; found, 1696.7373.

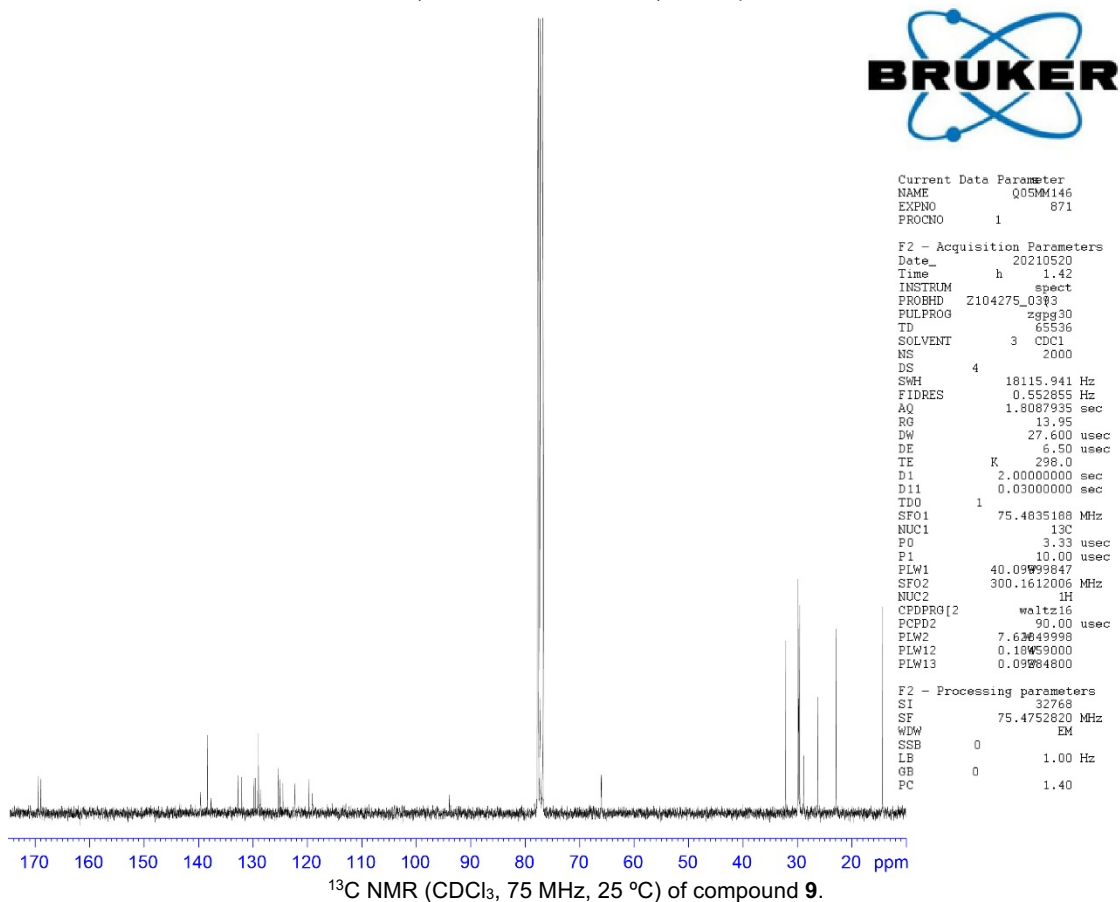
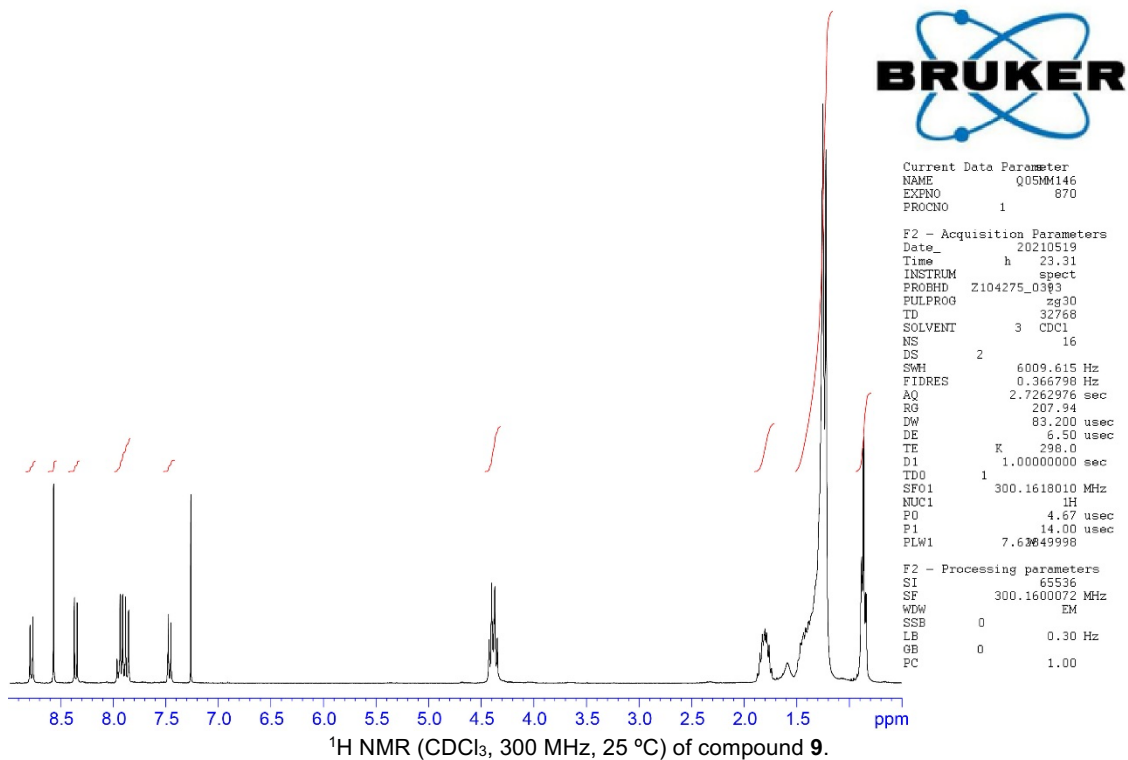
5-(4''-(2-(2-(2-methoxyethoxy)ethoxy)ethoxy)ethoxy)-[1,1':4',1''-terphenyl]-4-yl)-2,8-bis(3,4,5-tris(2-(2-(2-methoxyethoxy)ethoxy)ethoxy)phenyl)-1*H*-pyrido[3',4':5':4,5]naphtho[2,1,8-*cde*]pyrido[3',4':5':4,5]naphtho[8,1,2-*ghi*]isoindole-1,3,7,9(2*H*,5*H*,8*H*)-tetraone (4)

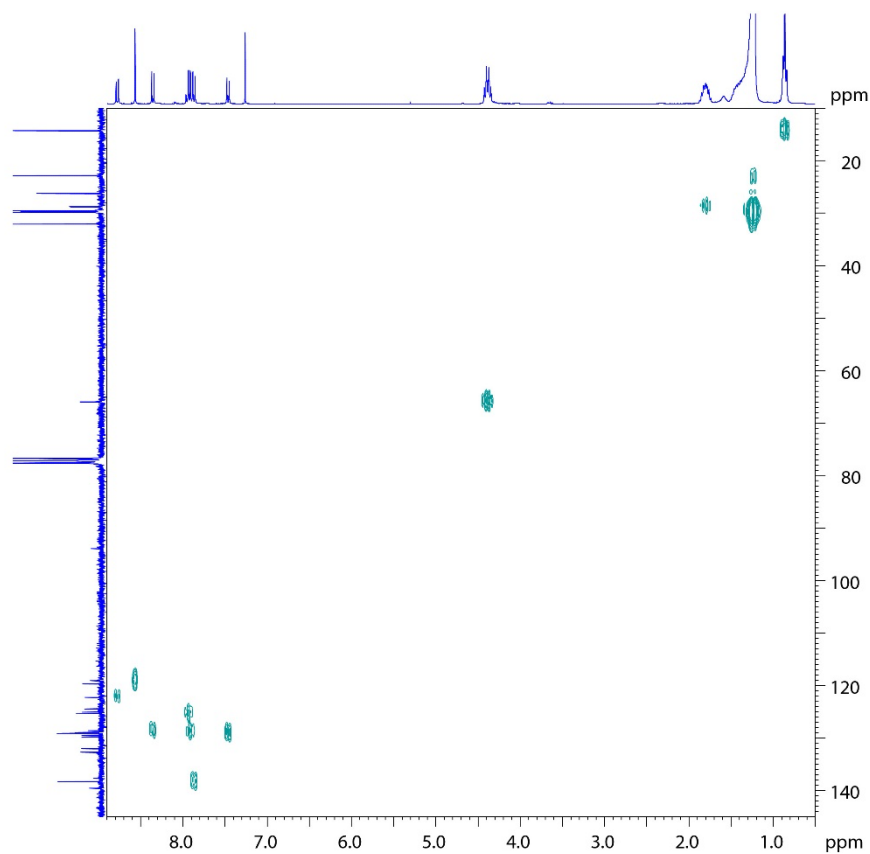


C<sub>103</sub>H<sub>127</sub>N<sub>3</sub>O<sub>32</sub>  
 Exact Mass: 1917.8403  
 Mol. Wt.: 1919.1114

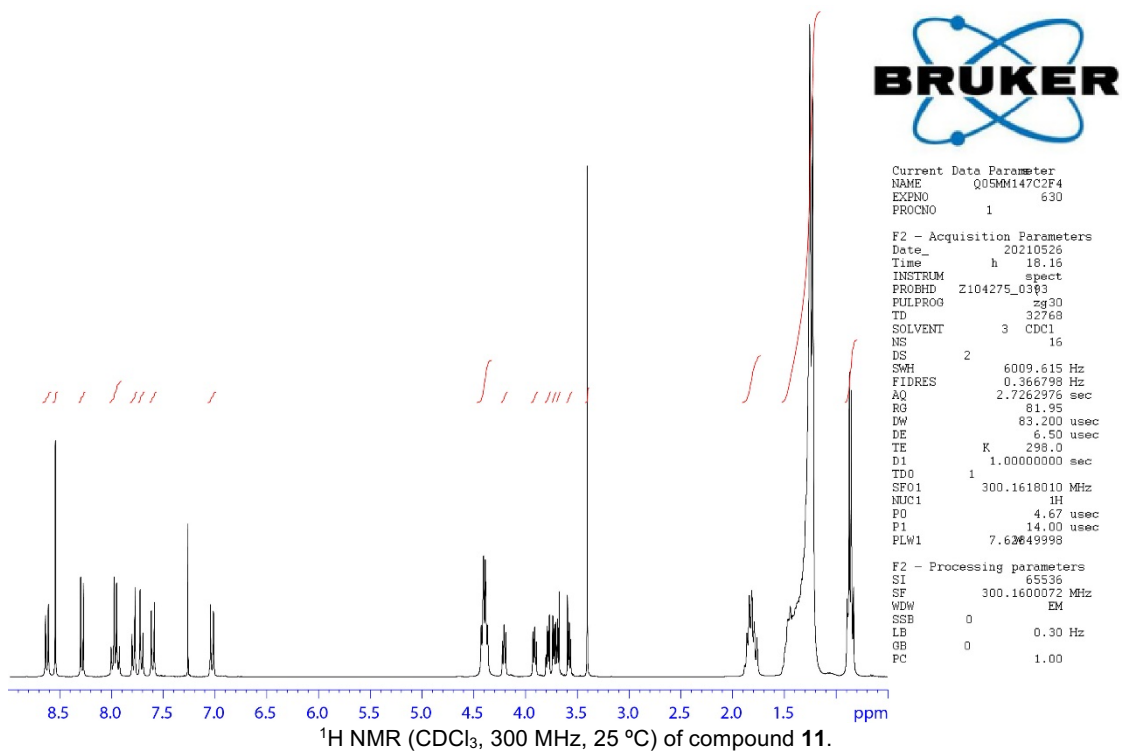
Compound **4** was obtained after column chromatography purification (silica gel, CHCl<sub>3</sub>/MeOH 10/0.3) as a viscous red solid (49 mg, 39 %). <sup>1</sup>H NMR (CDCl<sub>3</sub>, 500 MHz) δ/ppm 8.83 (2H, H<sub>3</sub>, s), 8.63 (2H, H<sub>1</sub>, d, *J* = 8.0 Hz), 8.51 (2H, H<sub>2</sub>, d, *J* = 8.0 Hz), 8.02 (2H, H<sub>6</sub>, d, *J* = 8.4 Hz), 7.82 (2H, H<sub>5</sub>, d, *J* = 8.4 Hz), 7.78 (2H, H<sub>7</sub>, d, *J* = 8.4 Hz), 7.70 (2H, H<sub>8</sub>, d, *J* = 8.4 Hz), 7.59 (2H, H<sub>9</sub>, d, *J* = 8.8 Hz), 7.03 (2H, H<sub>10</sub>, d, *J* = 8.8 Hz), 6.79 (4H, H<sub>4</sub>, s), 4.28 (4H, H<sub>a</sub>, t, *J* = 5.2 Hz), 4.22 (2H, H<sub>h</sub>, t, *J* = 5.0 Hz), 4.09 (8H, H<sub>a</sub>, br), 3.93 – 3.87 (6H, H<sub>b+i</sub>, m), 3.82 – 3.76 (10H, H<sub>b+i</sub>, m), 3.75 – 3.67 (22H, H<sub>c+c'+d+k</sub>, m), 3.66 – 3.55 (22H, H<sub>d'+e+e'+f+i</sub>, m), 3.54 – 3.52 (2H, H<sub>m</sub>, m), 3.52 – 3.48 (8H, H<sub>f</sub>, m), 3.40 (6H, H<sub>g'</sub>, s), 3.39 (3H, H<sub>n</sub>, s), 3.32 (12H, H<sub>g</sub>, s). <sup>13</sup>C NMR (CDCl<sub>3</sub>, 125 MHz) δ/ppm 164.6, 163.4, 158.8, 153.2, 141.0, 140.7, 138.2, 137.5, 136.2, 133.6, 133.1, 132.3, 131.2, 129.4, 128.2, 127.6, 127.4, 125.1, 124.3, 123.9, 122.6, 121.6, 121.0, 119.6, 115.2, 108.4, 72.6, 72.0(9), 72.0(7), 72.0(3), 72.0(0), 71.0, 70.8(1), 70.8(0), 70.7(9), 70.7(5), 70.7(1), 70.6(7), 70.6(5), 70.5(8), 69.9, 69.7, 68.9, 67.7, 59.2, 59.1(4), 59.0(7). FTIR (neat) 628, 667, 698, 711, 725, 740, 804, 822, 849, 945, 1004, 1109, 1182, 1199, 1245, 1303, 1363, 1391, 1422, 1436, 1455, 1472, 1493, 1532, 1559, 1602, 1663, 1698, 2873, 2922 cm<sup>-1</sup>. HRMS (MALDI-TOF, exact mass) calcd. for C<sub>103</sub>H<sub>127</sub>N<sub>3</sub>O<sub>32</sub> [M+Na]<sup>+</sup>, 1940.8300; found, 1940.8279.

### 3.- Collection of spectra

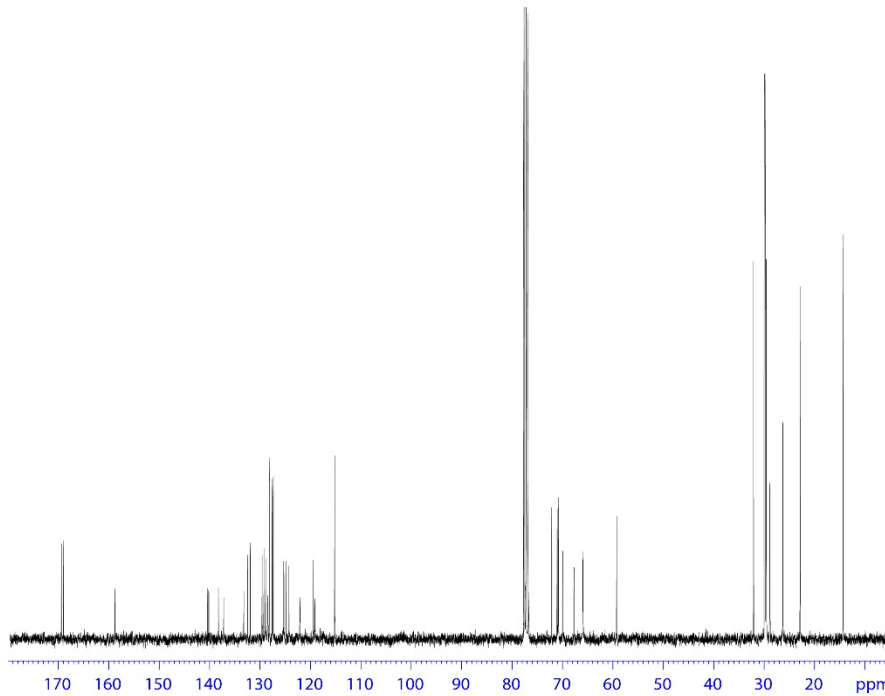




$^1\text{H}$ ,  $^{13}\text{C}$ -HMBC spectrum ( $\text{CDCl}_3$ , 25 °C) of compound **9**.



$^1\text{H}$  NMR ( $\text{CDCl}_3$ , 300 MHz, 25 °C) of compound **11**.

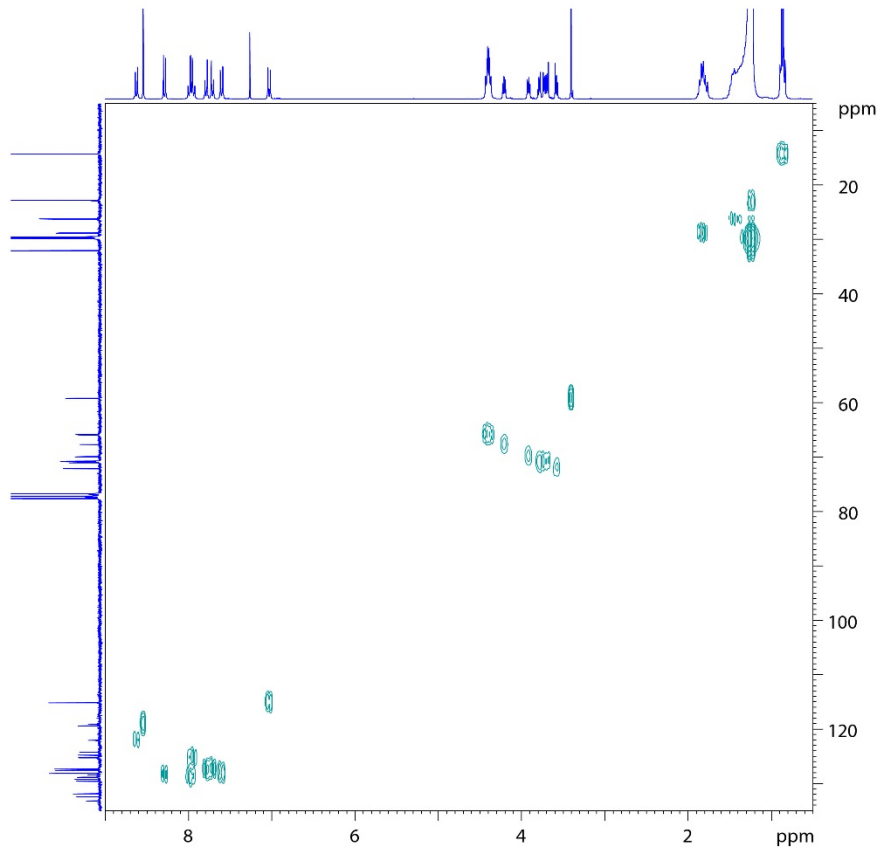


Current Data Parameter  
NAME Q05MM147C2F4  
EXPNO 631  
PROCNO 1

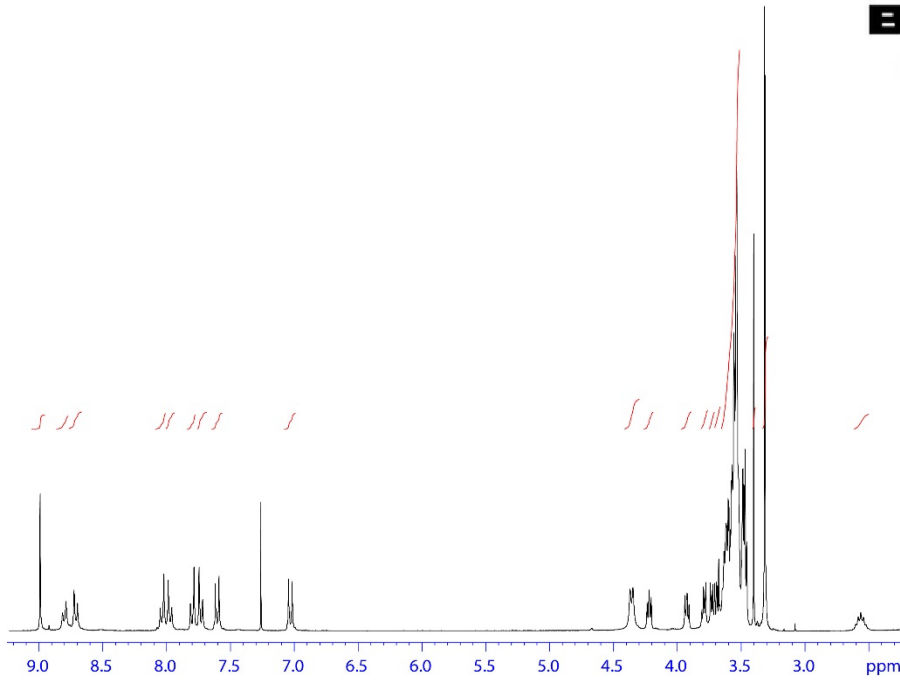
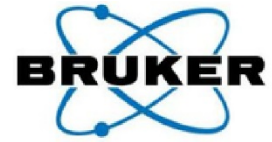
F2 - Acquisition Parameters  
Date\_ 20210526  
Time h 19.09  
INSTRUM spect  
PROBHD Z104275\_0303  
PULPROG zgpg30  
TD 65536  
SOLVENT 3 CDCl  
NS 800  
DS 4  
SWH 18115.941 Hz  
FIDRES 0.552855 Hz  
AQ 1.8087935 sec  
RG 13.95  
Dw 27.600 usec  
DE 6.50 usec  
TE K 298.0  
D1 2.0000000 sec  
D11 0.0300000 sec  
TD0 1  
SFO1 75.4835188 MHz  
NUC1 13C  
P0 3.33 usec  
P1 10.00 usec  
PLW1 40.09099847  
SFO2 300.1612006 MHz  
NUC2 1H  
CPDPRG2 waltz16  
PCPD2 90.00 usec  
PLW2 7.63849998  
PLW12 0.18059000  
PLW13 0.09004800

F2 - Processing parameters  
SI 32768  
SF 75.4752848 MHz  
WDW EM  
SSB 0  
LB 1.00 Hz  
GB 0  
PC 1.40

$^{13}\text{C}$  NMR ( $\text{CDCl}_3$ , 75 MHz, 25  $^\circ\text{C}$ ) of compound 11.



$^1\text{H}$ ,  $^{13}\text{C}$ -HMQC spectrum ( $\text{CDCl}_3$ , 25  $^\circ\text{C}$ ) of compound 11.

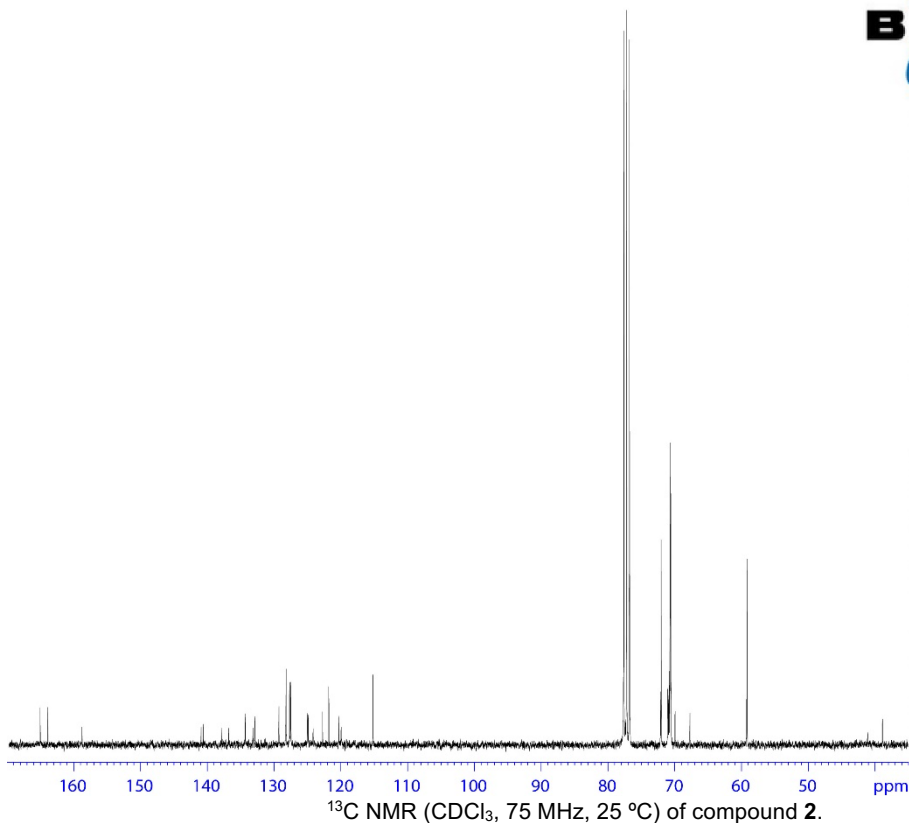


<sup>1</sup>H NMR (CDCl<sub>3</sub>, 300 MHz, 25 °C) of compound 2.

```
Current Data Parameter
NAME      Q05MM149C13
EXPNO     510
PROCNO    1

F2 - Acquisition Parameters
Date_     20210604
Time      h 21.22
INSTRUM   spect
PROBHD    Z104275_0303
FULPROG   zg30
TD        32768
SOLVENT   3  CDCl3
NS        16
DS        2
SWH       6009.615 Hz
FIDRES    0.366798 Hz
AQ        2.7262976 sec
RG        207.94
DW        83.200 usec
DE        6.50 usec
TE        K 298.0
D1        1.00000000 sec
TDO       1
SF01      300.1618010 MHz
NUC1      1H
P0        4.67 usec
P1        14.00 usec
PLW1      7.62649998

F2 - Processing parameters
SI        65536
SF        300.1600073 MHz
WDW       EM
SSB       0
LB        0.30 Hz
GB        0
PC        1.00
```

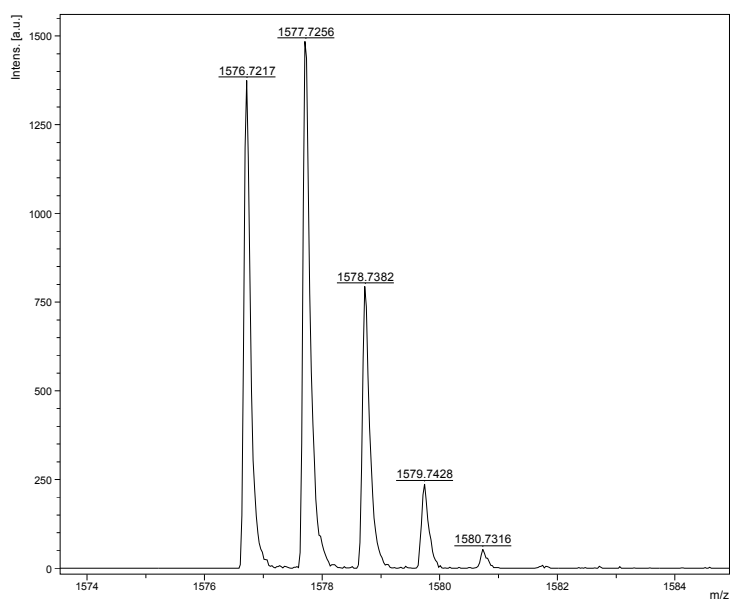
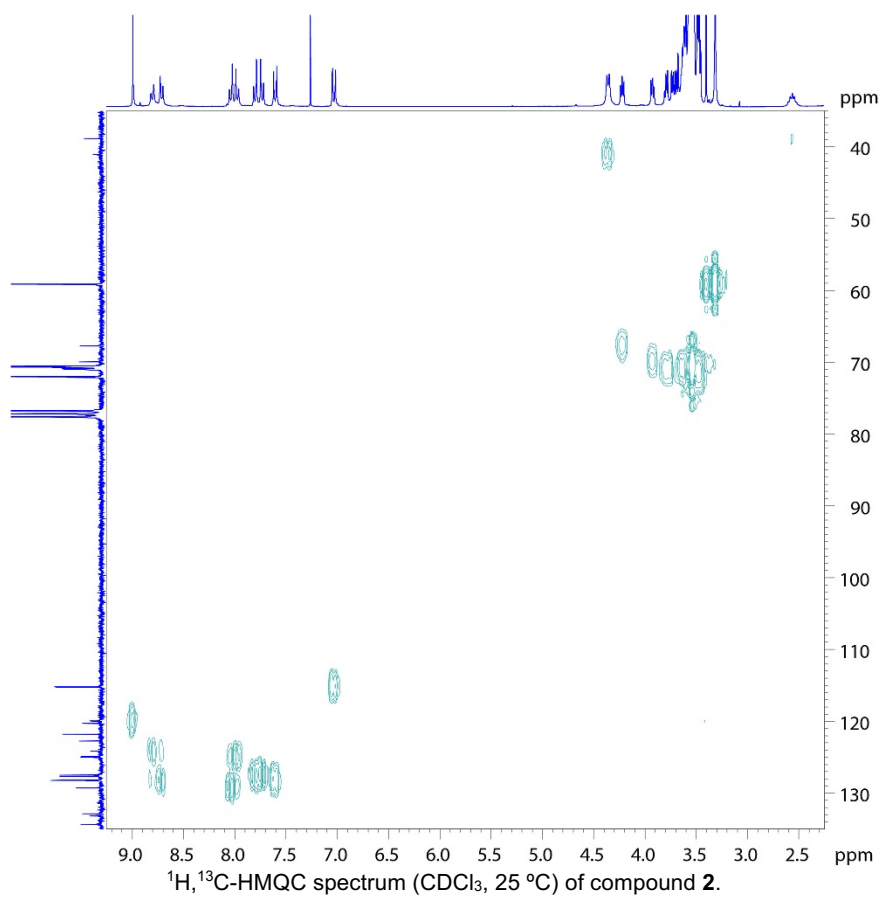


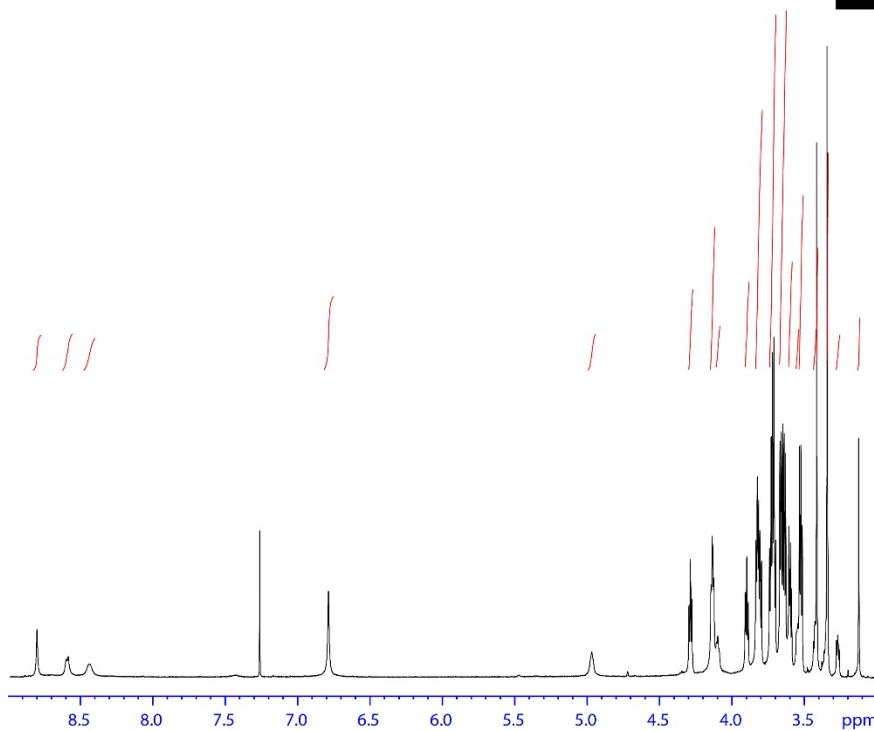
<sup>13</sup>C NMR (CDCl<sub>3</sub>, 75 MHz, 25 °C) of compound 2.

```
Current Data Parameters
NAME      Q05MM149C13
EXPNO     511
PROCNO    1

F2 - Acquisition Parameter
Date_     20210604
Time      h 23.33
INSTRUM   spect
PROBHD    Z104275_0303
FULPROG   zgpg30
TD        85536
SOLVENT   3  CDCl3
NS        2000
DS        4
SWH       18115.941 Hz
FIDRES    0.552855 Hz
AQ        1.8087935 sec
RG        13.95
DW        27.600 usec
DE        6.50 usec
TE        K 298.0
D1        2.00000000 sec
D11       0.03000000 sec
TDO       1
SF01      75.4835188 MHz
NUC1      13C
P0        3.33 usec
P1        10.00 usec
PLW1      40.09999847
SF02      300.1612006 MHz
NUC2      1H
CPDPRG[2] waltz16
PCPD2     90.00 usec
PLW2      7.62649998
PLW12     0.10459000
PLW13     0.09284800

F2 - Processing parameter
SI        32768
SF        75.4752843 MHz
WDW       EM
SSB       0
LB        1.00 Hz
GB        0
PC        1.40
```





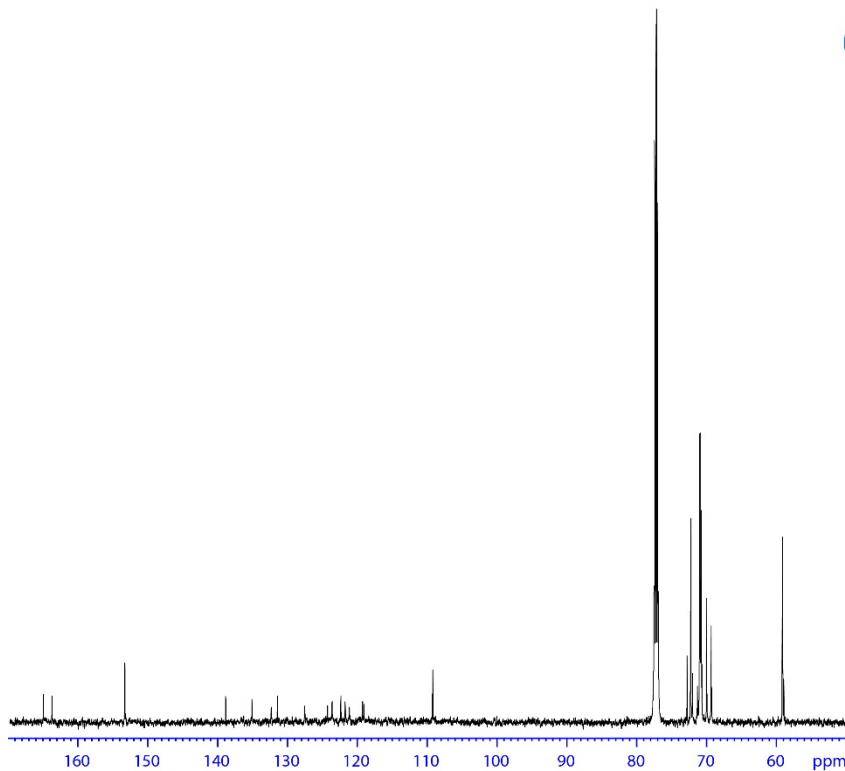
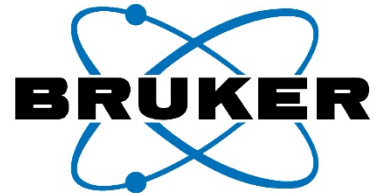
Current Data Parameters  
NAME Q05MM163\_500MHz  
EXPNO 1  
PROCNO 1

F2 - Acquisition Parameters  
Date\_ 20211027  
Time 13.22  
INSTRUM spect  
PROBHD 5 mm PATBO BB-  
PULPROG zg30  
TD 32768  
SOLVENT CDC13  
NS 4  
DS 2  
SWH 7507.507 Hz  
FIDRES 0.229111 Hz  
AQ 2.1823487 s  
RG 181  
DW 66.600 us  
DE 6.00 us  
TE K 323.0  
D1 1.0000000 s  
TD0 1

===== CHANNEL f1 =====  
NUC1 1H  
P1 15.00 us  
PL1 -5.20 dB  
PL1W 34.93W07822  
SFO1 500.1330008 MHz

F2 - Processing parameters  
SI 32768  
SF 500.1300127 MHz  
WDW EM  
SSR 0

<sup>1</sup>H NMR (CDCl<sub>3</sub>, 500 MHz, 50 °C) of compound 3.



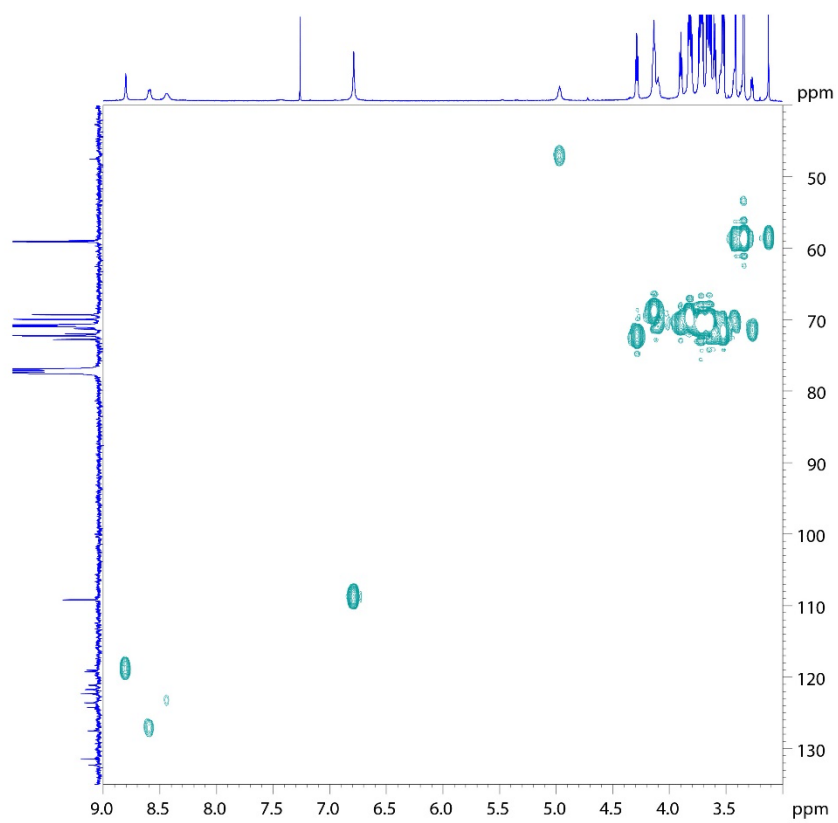
Current Data Parameters  
NAME Q05MM163\_500MHz  
EXPNO 2  
PROCNO 1

F2 - Acquisition Parameters  
Date\_ 20211027  
Time 13.27  
INSTRUM spect  
PROBHD 5 mm PATBO BB-  
PULPROG zgpg30  
TD 65536  
SOLVENT CDC13  
NS 2394  
DS 2  
SWH 31446.541 Hz  
FIDRES 0.479836 Hz  
AQ 1.0420223 s  
RG 20642.5  
DW 15.900 us  
DE 6.00 us  
TE K 323.0  
D1 2.0000000 s  
D11 0.0300000 s  
TD0 1

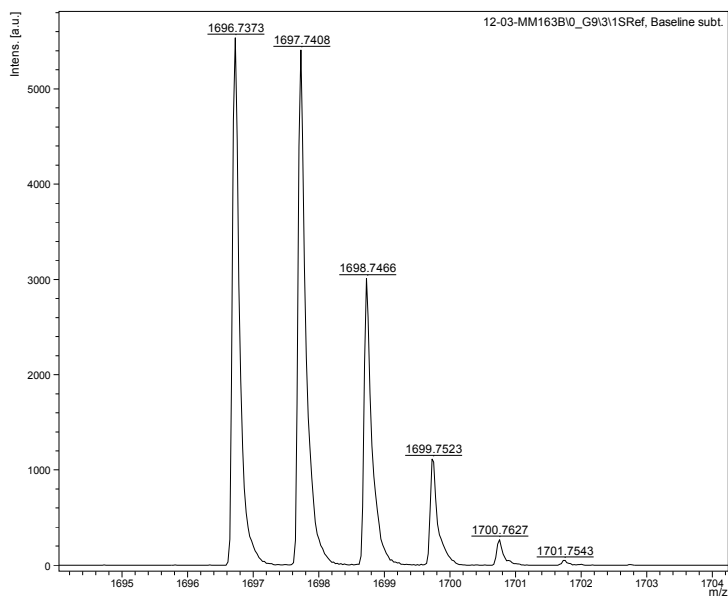
===== CHANNEL f1 =====  
NUC1 13C  
P1 9.25 us  
PL1 2.00 dB  
PL1W 46.91W83798  
SFO1 125.7722511 MHz

===== CHANNEL f2 =====  
CPDPRG[2] waltz16  
NUC2 1H  
PCPD2 80.000000 sec

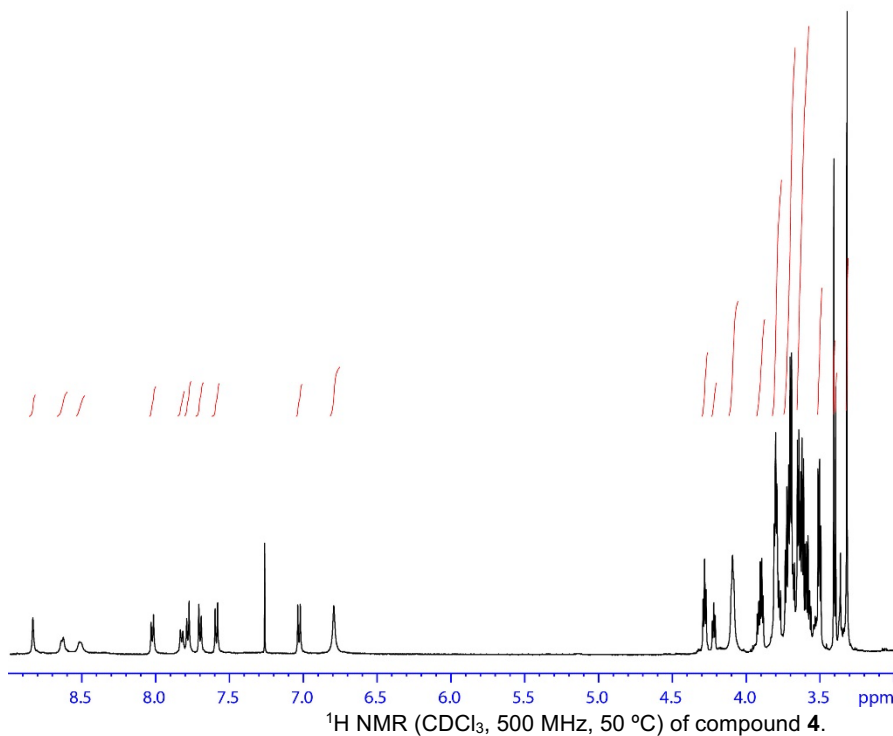
<sup>13</sup>C NMR (CDCl<sub>3</sub>, 125 MHz, 50 °C) of compound 3.



$^1\text{H}$ ,  $^{13}\text{C}$ -HMQC spectrum ( $\text{CDCl}_3$ ,  $50\text{ }^\circ\text{C}$ ) of compound **3**.



Mass spectrum of compound **3**.



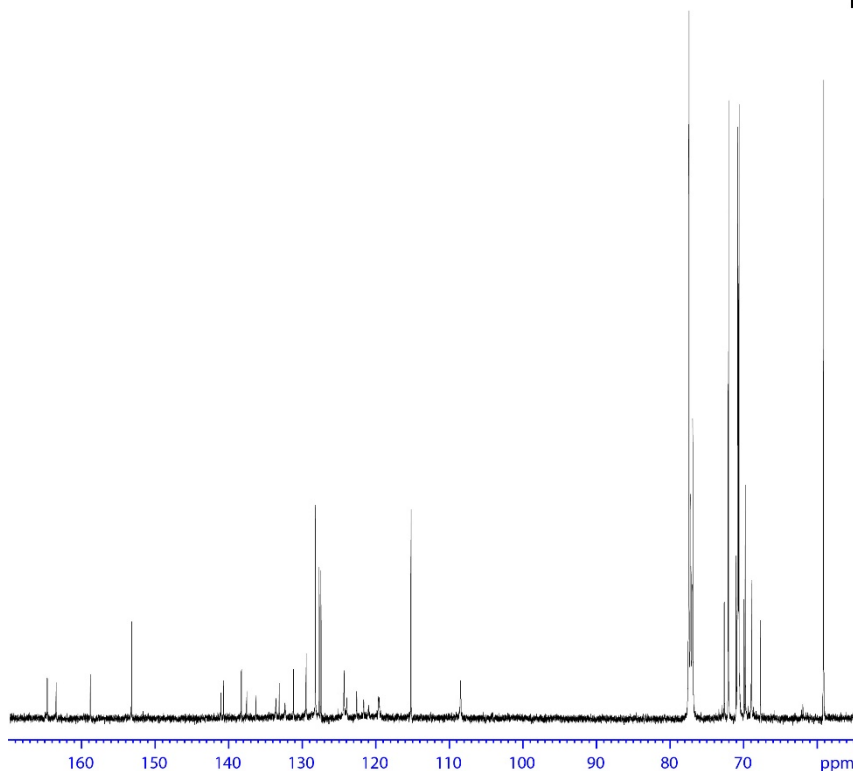
Current Data Parameters  
NAME Q05MM156-500MHz  
EXPNO 10  
PROCNO 1

F2 - Acquisition Parameters  
Date\_ 20210915  
Time 8.52  
INSTRUM spect  
PROBHD 5 mm PATBO BB-  
PULPROG zg30  
TD 32768  
SOLVENT CDCl3  
NS 4  
DS 2  
SWH 7507.507 Hz  
FIDRES 0.229111 Hz  
AQ 2.1823487 sec  
RG 128  
DW 66.600 usec  
DE 6.00 usec  
TE K 323.0  
D1 1.00000000 sec  
TDO 1

----- CHANNEL f1 -----  
NUC1 1H  
P1 15.00 usec  
PL1 -5.20 dB  
PL1W 34.93W07822  
SF01 500.1330008 MHz

F2 - Processing parameters  
SI 32768  
SF 500.1300129 MHz  
WDW EM  
SSB 0

<sup>1</sup>H NMR (CDCl<sub>3</sub>, 500 MHz, 50 °C) of compound 4.



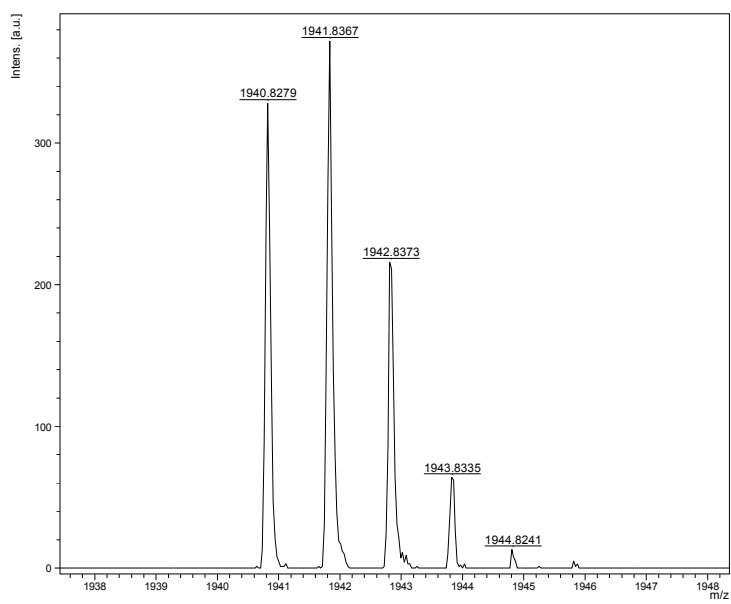
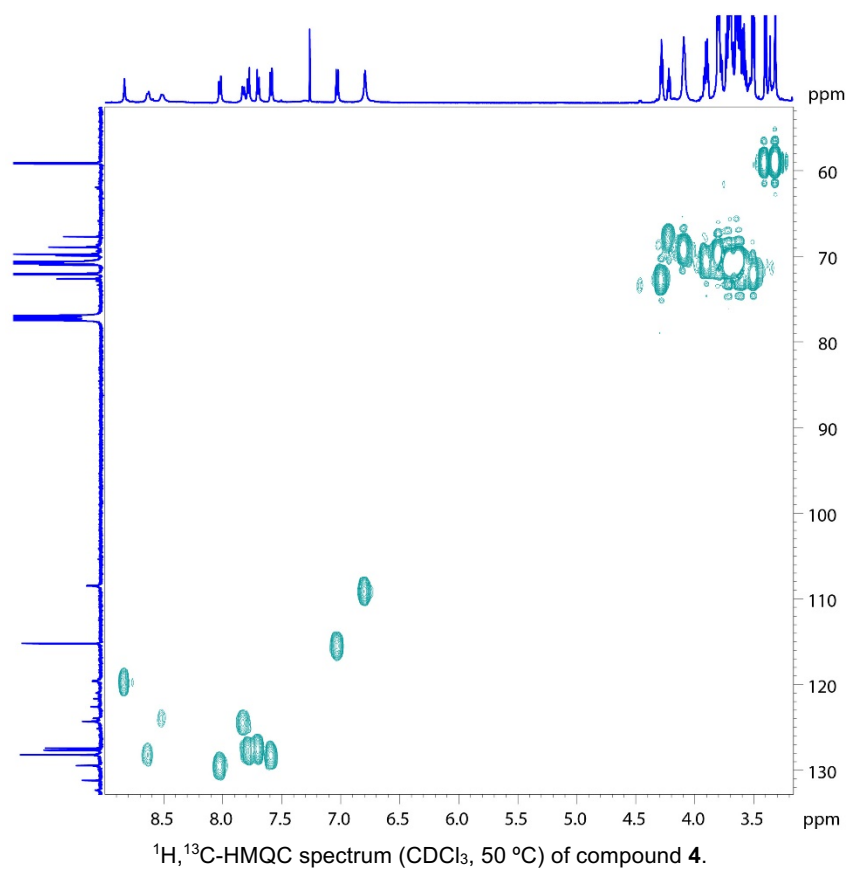
Current Data Parameters  
NAME Q05MM156-500MHz  
EXPNO 4  
PROCNO 1

F2 - Acquisition Parameters  
Date\_ 20210915  
Time 5.12  
INSTRUM spect  
PROBHD 5 mm PATBO BB-  
PULPROG zgpg30  
TD 85536  
SOLVENT CDCl3  
NS 10000  
DS 2  
SWH 31446.541 Hz  
FIDRES 0.479836 Hz  
AQ 1.0420223 sec  
RG 20642.5  
DW 15.900 usec  
DE 6.00 usec  
TE K 297.6  
D1 2.00000000 sec  
D11 0.03000000 sec  
TDO 1

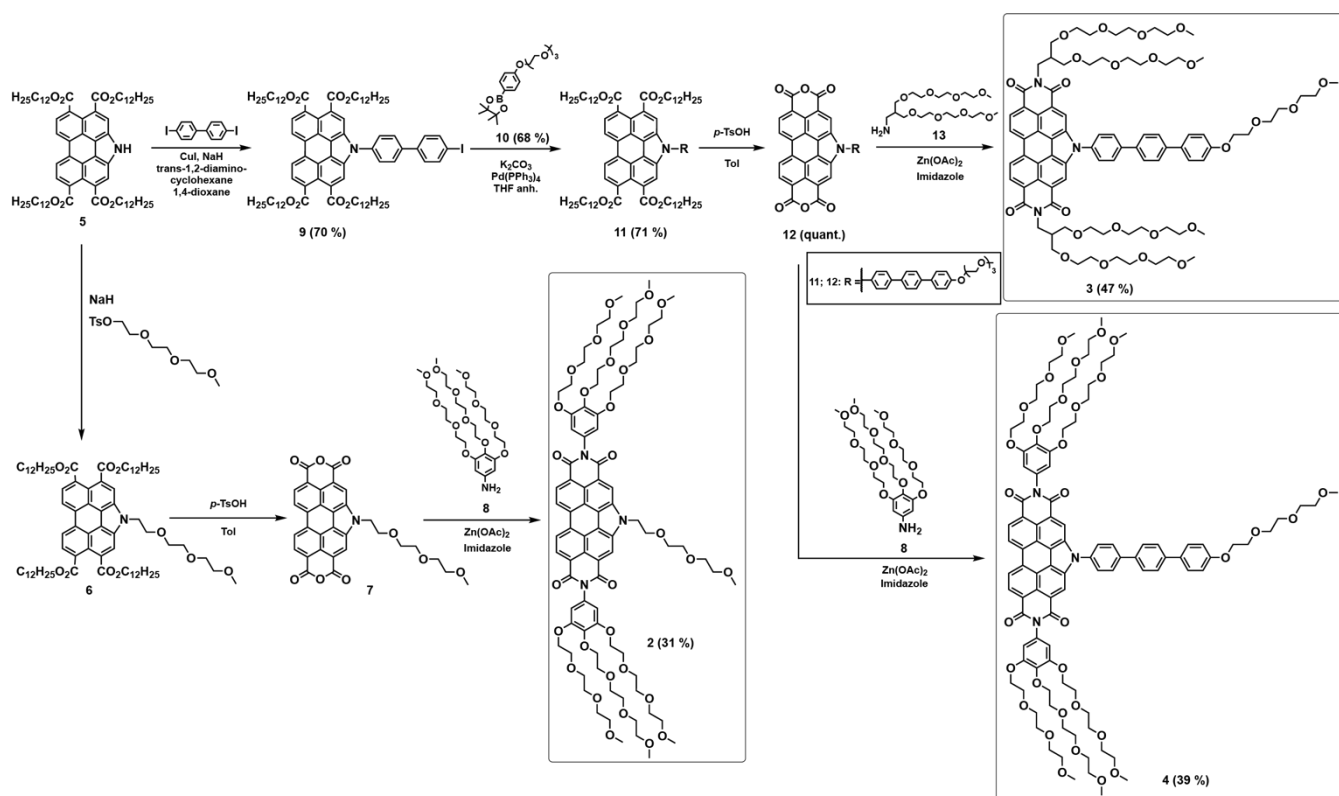
----- CHANNEL f1 -----  
NUC1 13C  
P1 9.25 usec  
PL1 2.00 dB  
PL1W 46.91W83798  
SF01 125.7722511 MHz

----- CHANNEL f2 -----  
CPDPRG[2] waltz16  
NUC2 1H  
PCPD2 80.00usec

<sup>13</sup>C NMR (CDCl<sub>3</sub>, 125 MHz, 50 °C) of compound 4.



#### 4.- Supplementary Figures and Tables



**Scheme S1.** Synthesis of amphiphilic *N*-annulated PBIs 2-4.

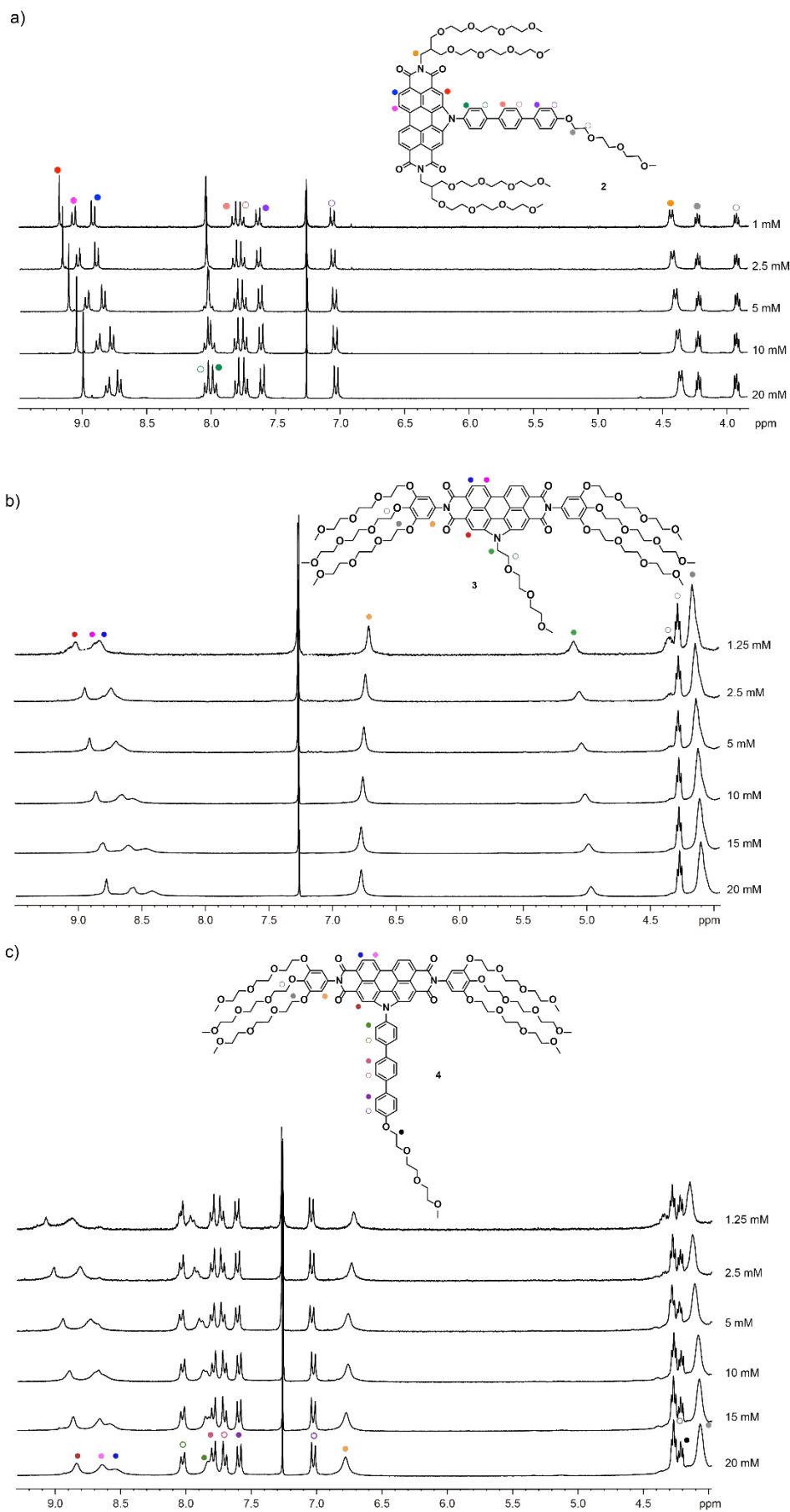
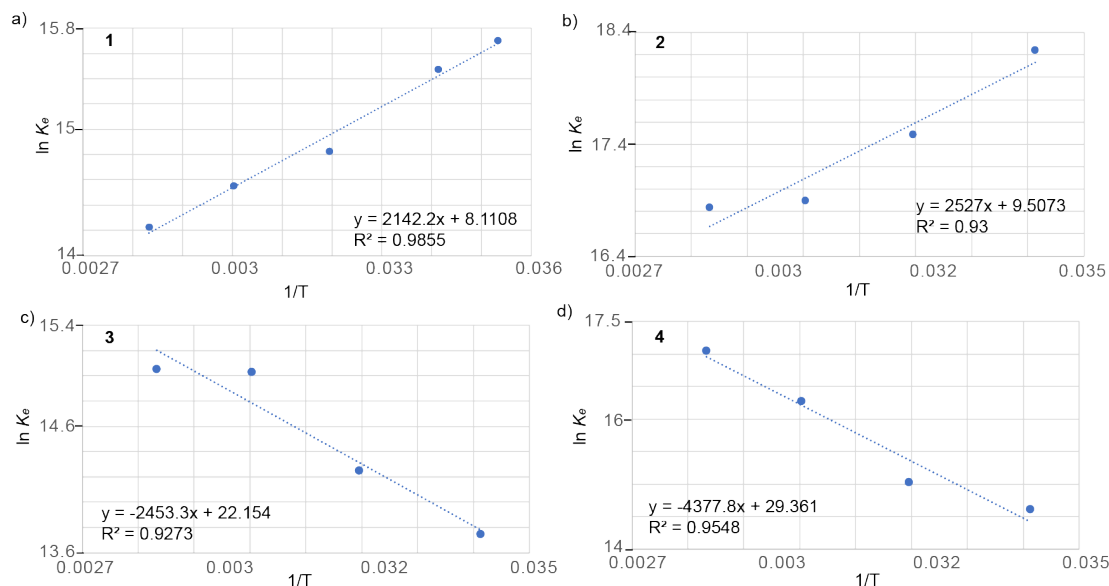
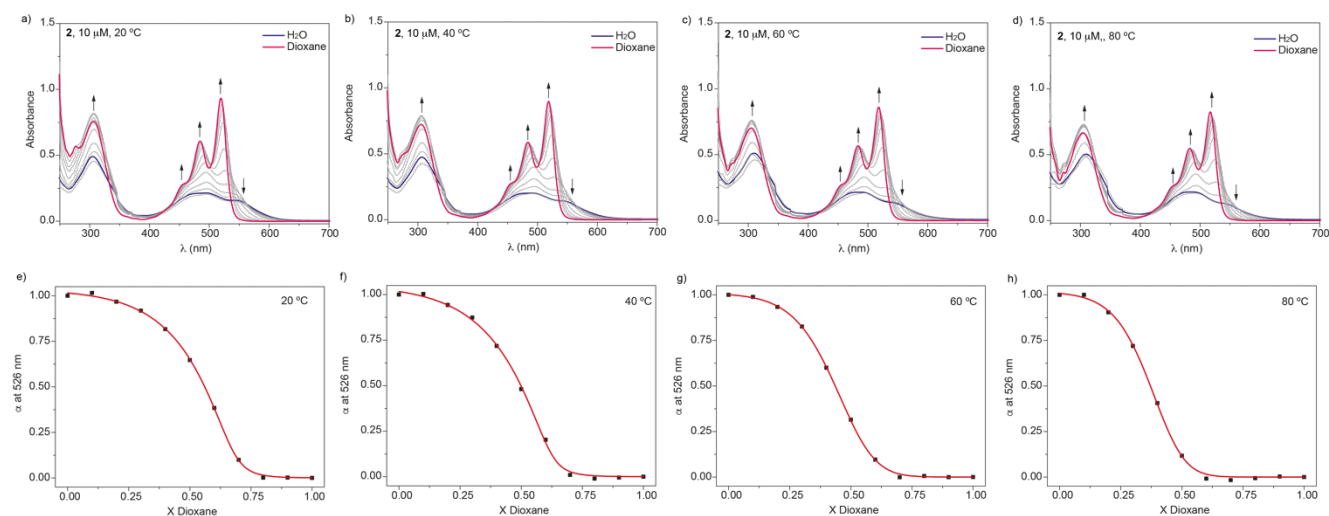


Figure S1. Partial  $^1\text{H}$  NMR spectra of amphiphiles 2-4 (300 MHz; 298 K;  $\text{CDCl}_3$ ).

**Table S1.** Thermodynamic parameters associated to the self-assembly of **1** in water ( $X_{\text{dioxane}} = 0$ ).

Temperature (°C)	$\Delta G$ (kJ mol <sup>-1</sup> )	$m$ (kJ mol <sup>-1</sup> )	$\sigma$ (-)
20	-37.7 ± 8	16.3	1
40	-38.5 ± 1	16.8	1
60	-40.3 ± 2	19.5	1
80	-41.7 ± 3	20.7	1

**Figure S2.** Van't Hoff plots for compounds **1–4** in water and at  $c_T = 10 \mu\text{M}$ . The inset in each panel collects the straight-line equation used to derive the values of  $\Delta H$  and  $\Delta S$ .**Figure S3.** (a-d) UV-Vis spectra of amphiphile **2** in water/dioxane mixtures at different temperatures and a  $c_T = 10 \mu\text{M}$ . Arrows in panels (a-d) indicate the changes in the UV-Vis spectra upon adding increasing amounts of dioxane. (e-h) Denaturation curves of **2** in water/dioxane mixtures at different temperatures. Red lines in panels (e-h) depict the fitting to the SD model.**Table S2.** Thermodynamic parameters associated to the self-assembly of **2** in water ( $X_{\text{dioxane}} = 0$ ).

Temperature (°C)	$\Delta G$ (kJ mol <sup>-1</sup> )	$m$ (kJ mol <sup>-1</sup> )	$\sigma$ (-)
20	-37.6 ± 6	14.7	$1.5 \times 10^{-2}$
40	-38.6 ± 1	14.5	$1.0 \times 10^{-2}$
60	-47.9 ± 2	32.5	1
80	-50.6 ± 5	40.1	1

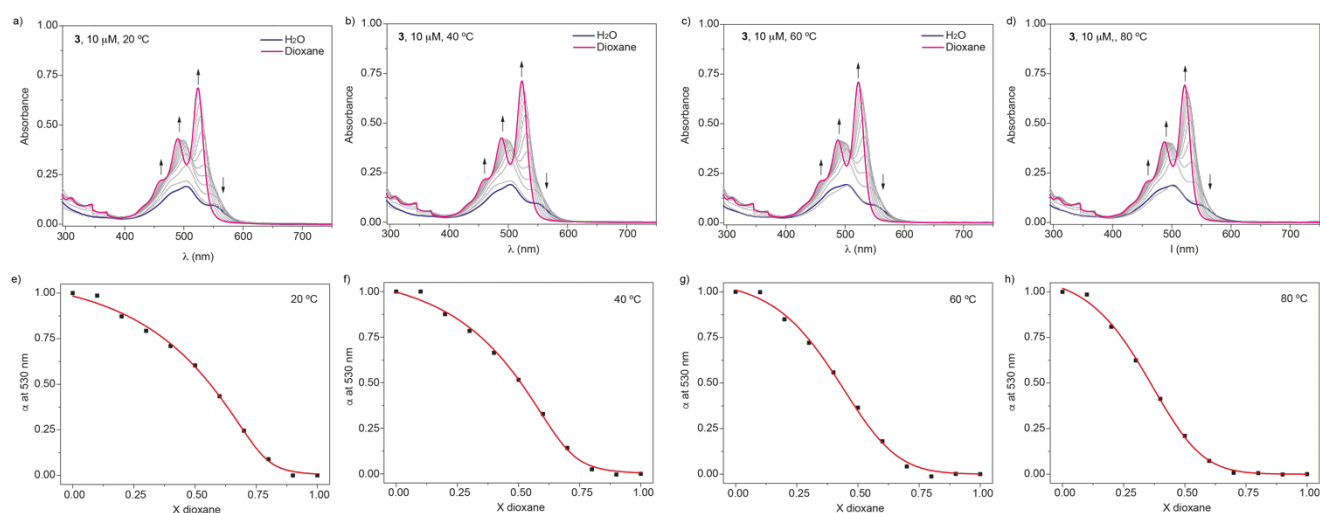


**Figure S4.** (a-d) UV-Vis spectra of amphiphile **3** in water/dioxane mixtures at different temperatures and a  $c_T = 10 \mu\text{M}$ . Arrows in panels (a-d) indicate the changes in the UV-Vis spectra upon adding increasing amounts of dioxane. (e-h) Denaturation curves of **3** in water/dioxane mixtures at different temperatures. Red lines in panels (e-h) depict the fitting to the SD model.

**Table S3.** Thermodynamic parameters associated to the self-assembly of **3** in water ( $X_{\text{dioxane}} = 0$ ).

Temperature ( $^{\circ}\text{C}$ )	$\Delta G$ ( $\text{kJ mol}^{-1}$ )	$m$ ( $\text{kJ mol}^{-1}$ )	$\sigma$ (-)
20	$-33.5 \pm 1$	7.3	$4.9 \times 10^{-3}$
40	$-37.1 \pm 2$	9.5	$1.6 \times 10^{-2}$
60	$-41.6 \pm 3$	21.5	1
80	$-44.1 \pm 8$	24.5	1

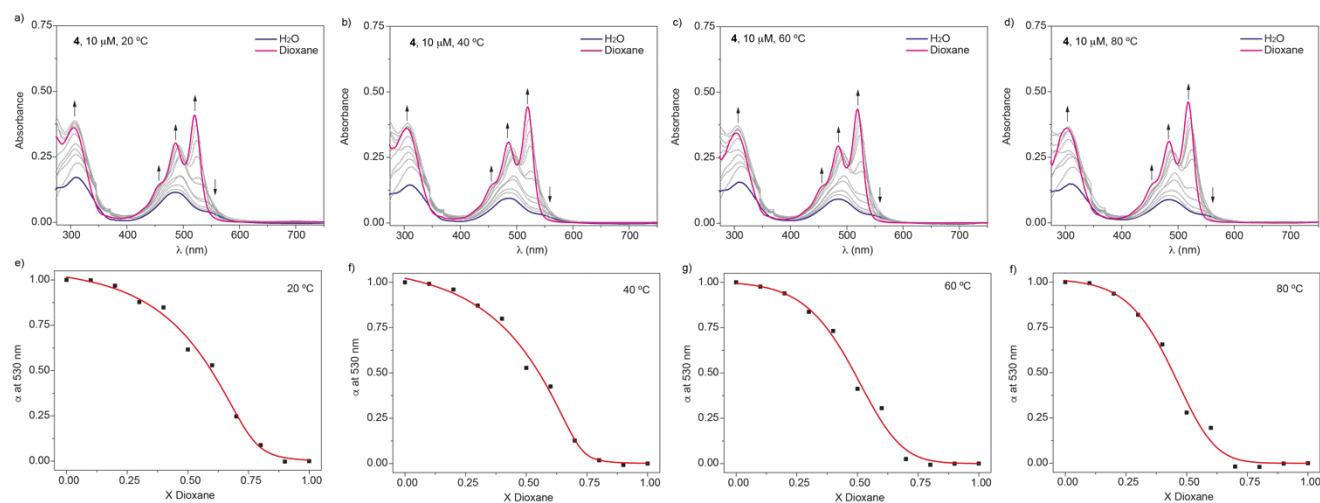


**Figure S5.** (a-d) UV-Vis spectra of amphiphile **4** in water/dioxane mixtures at different temperatures and a  $c_T = 10 \mu\text{M}$ . Arrows in panels (a-d) indicate the changes in the UV-Vis spectra upon adding increasing amounts of dioxane. (e-h) Denaturation curves of **4** in water/dioxane mixtures at different temperatures. Red lines in panels (e-h) depict the fitting to the SD model.

**Table S4.** Thermodynamic parameters associated to the self-assembly of **4** in water ( $X_{\text{dioxane}} = 0$ ).

Temperature ( $^{\circ}\text{C}$ )	$\Delta G$ ( $\text{kJ mol}^{-1}$ )	$m$ ( $\text{kJ mol}^{-1}$ )	$\sigma$ (-)
20	$-33.6 \pm 1$	10.4	$1.3 \times 10^{-2}$
40	$-39.1 \pm 1$	10.3	$3.2 \times 10^{-3}$
60	$-45.8 \pm 14$	27.2	1
80	$-50.0 \pm 16$	32.2	1

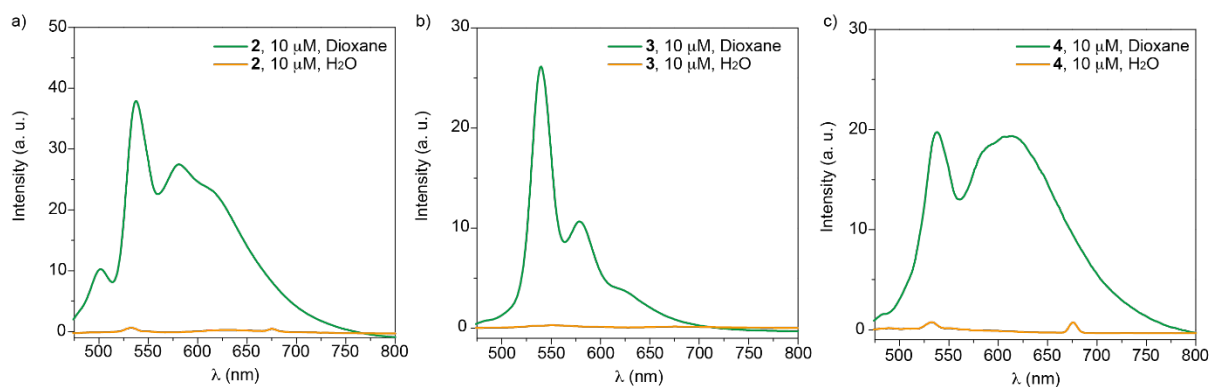


**Figure S6.** (a-c) Emission spectra of **2-3** in water (orange line) and dioxane (green line) ( $\lambda_{\text{exc}} = 493 \text{ nm}$ ;  $c_T = 10 \mu\text{M}$ ).

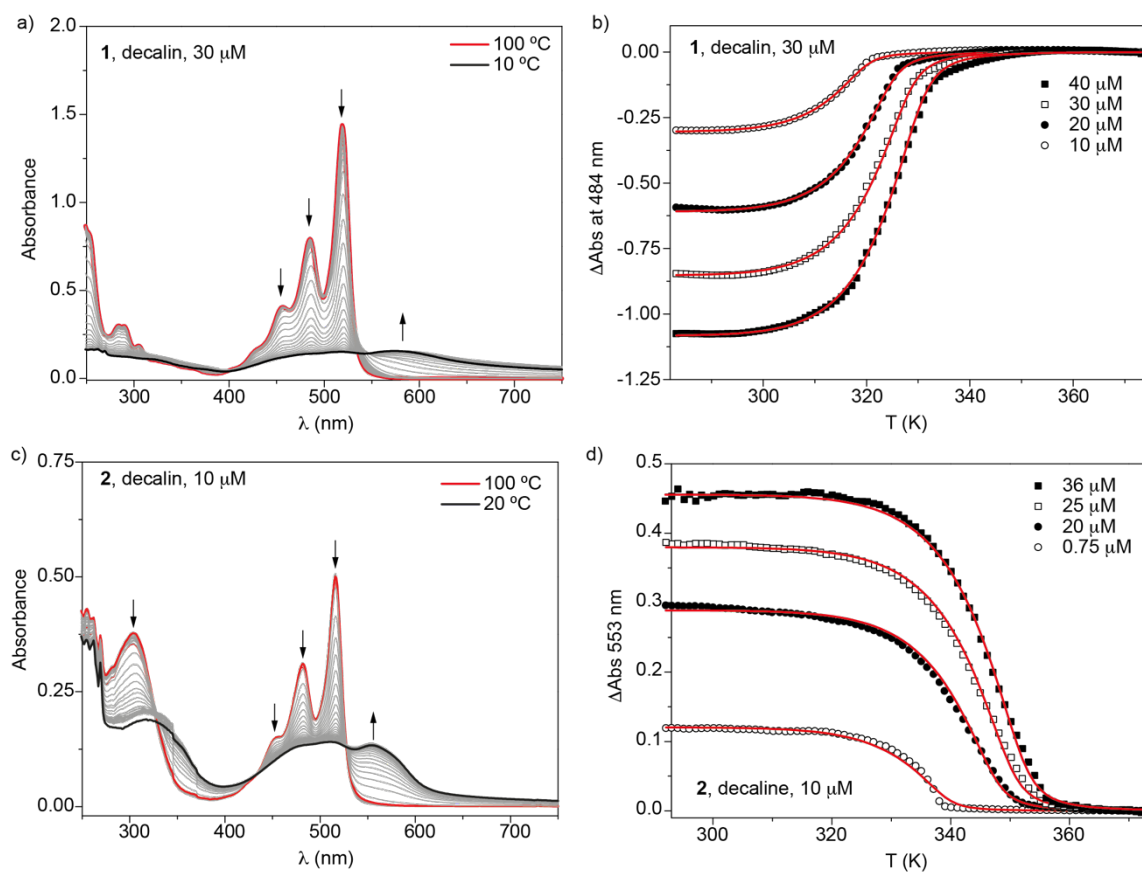


**Figure S7.** UV-Vis spectra of **1** (a) and **2** (c) at different temperatures in decalin as solvent. Arrows indicate the changes in the absorption bands upon decreasing the temperature. Cooling curves ( $1 \text{ K min}^{-1}$ ) of **1** (b) and **2** (d) in decalin at different concentrations. Red lines in (b) and (d) depict the fitting to the one-component EQ model.

**Table S5.** Thermodynamic parameters associated to the self-assembly of **1** and **2** in decalin at 293 K.

	$\Delta H_e$ (kJ·mol <sup>-1</sup> )	$\Delta H_n$ (kJ mol <sup>-1</sup> )	$\Delta S$ (J K <sup>-1</sup> mol <sup>-1</sup> )	$\Delta G$ (kJ mol <sup>-1</sup> )	$K_e$ (M <sup>-1</sup> )	$K_n$ (M <sup>-1</sup> )	$\sigma$ (-)
<b>1</b>	$-113.9 \pm 1$	$-9.9 \pm 1$	$-262 \pm 2$	$-37.1 \pm 1$	$1.9 \times 10^6$	$3.6 \times 10^4$	$1.8 \times 10^{-2}$
<b>2</b>	$-122.5 \pm 2$	$-12.0 \pm 1$	$-264 \pm 3$	$-45.1 \pm 2$	$4.9 \times 10^7$	$3.7 \times 10^5$	$7.6 \times 10^{-3}$

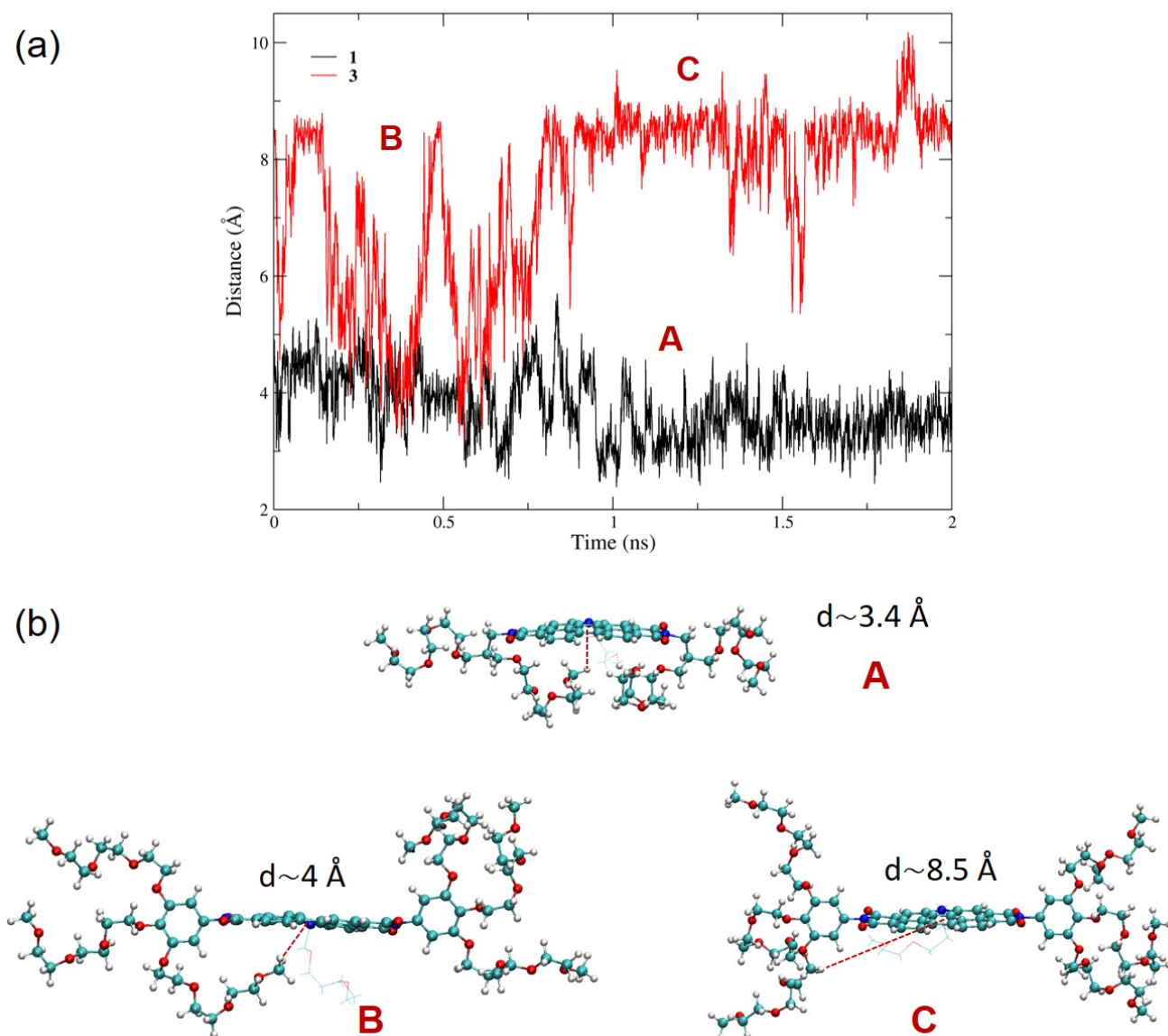


**Figure S8.** a) Minimum distance between the centroid of the central benzene ring of the *N*-PBI core and any atom of the terminal OEG chains on the imide positions along the MD trajectories of monomers 1 (black) and 3 (red) in water. b) Representative structures of 1 (A) and 3 (B and C) along the MD trajectories.

## Discussion on the monomer energetics

As discussed on the main text, the chain-core, core-solvent and chain-solvent interactions ( $\overline{E}_{pot}^{c-ch}$ ,  $\overline{E}_{pot}^{c-solv}$  and  $\overline{E}_{pot}^{ch-solv}$ ) for monomers of **1** and **3** have been evaluated and their values are shown in Table S6. Table S6 reveals that the chain-core interactions are stronger for **1** (-53 kJ/mol) compared to **3** (-12 kJ/mol), which is in line with the more rigidity of the side chains in **3** where the OEG segments cannot effectively cover and protect the hydrophobic *N*-PBI core with chain-core distances larger than those found for **1** along the MD trajectories (Figure S8). The hydrophobic *N*-PBI skeleton of **3** is therefore more exposed to the solvent with an average of 24 water molecules in close contact with the *N*-PBI core (Table S6). This is the reason why the  $\overline{E}_{pot}^{c-solv}$  term for **3** (-239 kJ/mol) is slightly higher than that computed for **1** (-195 kJ/mol). Finally, the most important interaction is the chain-solvent contribution with a significant difference between **1** and **3** (-831 and -1192 kJ/mol, respectively) in concordance with the larger number of stabilizing water-OEG chain contacts for **3** compared to **1** (i.e., larger number of H-bonds between OEG chains and water, see Table S8). The self-assembly of **3** would therefore require the rupture of a larger number of stabilizing water-OEG chain and water-core interactions and it can explain the origin of the enthalpically unfavourable self-assembly process for **3** compared to **1**.

**Table S6.** Average chain-core, core-solvent and chain-solvent interactions ( $\overline{E}_{pot}^{c-ch}$ ,  $\overline{E}_{pot}^{c-solv}$  and  $\overline{E}_{pot}^{ch-solv}$ ) in kJ/mol computed for *N*-PBI **1** and **3** from the MD run. Last column includes the average number of water molecules within a distance of 4 Å with respect to the *N*-PBI cores during the MD trajectory.

Compound	$\overline{E}_{pot}^{c-ch}$	$\overline{E}_{pot}^{c-solv}$	$\overline{E}_{pot}^{ch-solv}$	Number of H <sub>2</sub> O
<i>N</i> -PBI <b>1</b>	-53	-195	-831	19
<i>N</i> -PBI <b>3</b>	-12	-239	-1192	24

## MD of dimers and tetramers

**Table S7.** Average length and estimated error of the cubic box edge used along the production stage of the MD simulation for energy calculations of the tetramer, dimer, and monomer. All quantities are expressed in nm.

Compound	Tetramer	Dimer	Monomer
<i>N</i> -PBI 1	7.4975 ± 0.0003	5.95034 ± 0.00012	4.72358 ± 0.00016
<i>N</i> -PBI 3	8.69045 ± 0.00011	6.89793 ± 0.00018	5.47445 ± 0.00018

**Table S8.** Average kinetic ( $T$ ), and  $pV$  energy terms (in kJ/mol) and their estimated errors calculated for the whole system from the trajectory of *N*-PBIs 1 and 3 dimers and monomers. The energy difference ( $\Delta E$ ) with respect to the equivalent number of monomers is also shown.

<i>N</i> -PBI 1			
Energy	Dimer	Monomer	$\Delta E$
$T$	61691 ± 4	30847 ± 3	-2.7
$pV$	12.6876 ± 0.0008	6.34697 ± 0.0007	-0.0063
<i>N</i> -PBI 3			
Energy	Dimer	Monomer	$\Delta E$
$T$	95866 ± 7	47923 ± 2	19.5
$pV$	19.7655 ± 0.0016	9.8804 ± 0.0010	0.0047

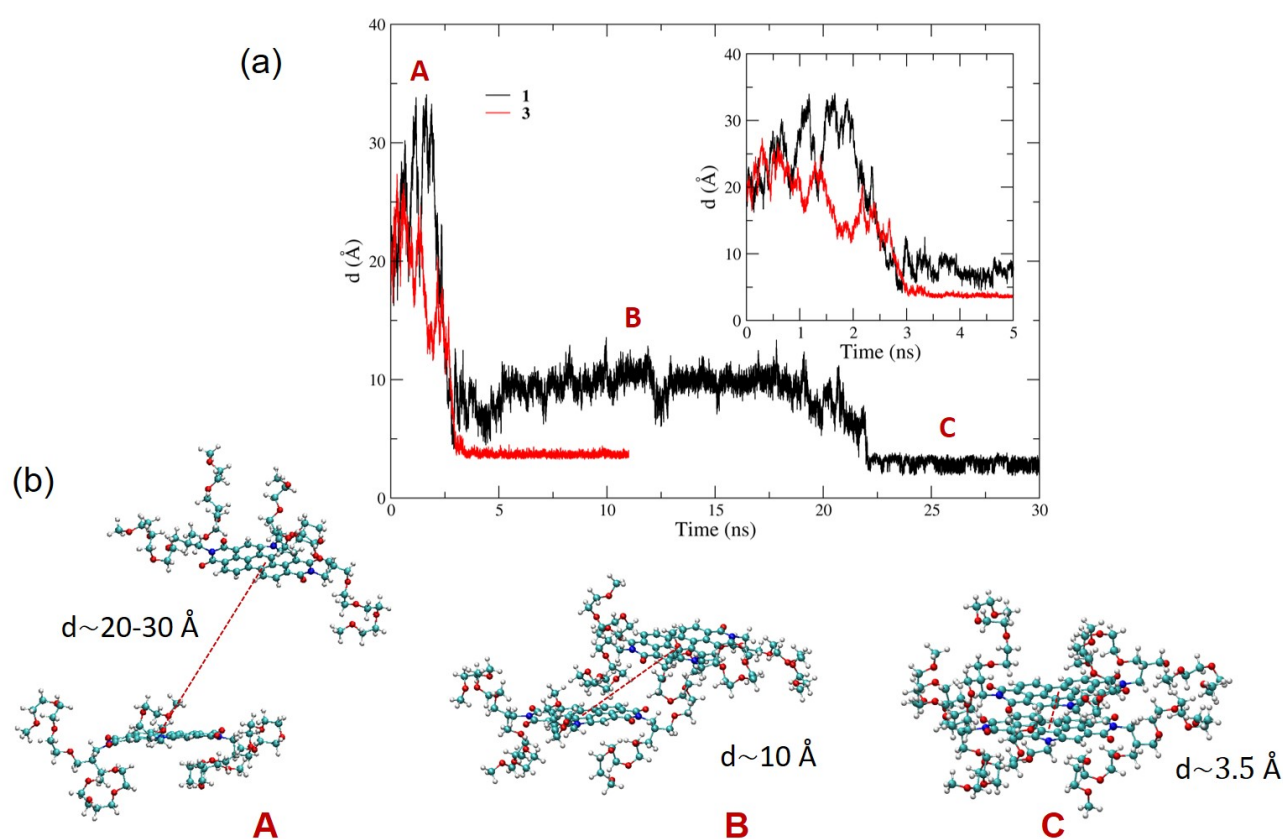


**Figure S9.** a) Distance between the centroids of the central benzene rings of the *N*-PBI cores ( $d$ ) along the MD trajectories for *N*-PBI dimers of 1 (black) and 3 (red) in water. The two monomers were initially separated by 20 Å. The inset highlights the first 5 ns of the simulations. b) Structures A, B, and C correspond to representative dispositions of the two monomers in the *N*-PBI dimer of 1 along the MD trajectory.

**Table S9.** Average number of H-bonds per monomeric unit between the side OEG chains and the water molecules calculated along the MD trajectory for supramolecular aggregates (dimer and tetramers) of *N*-PBIs 1 and 3 compared to the monomer.

Species	<i>N</i> -PBI 1		<i>N</i> -PBI 3	
	H-bonds	Lost H-bonds	H-bonds	Lost H-bonds
Monomer	20.0	–	27.9	–
Dimer	18.5	1.5	25.2	2.7
Tetramer	16.9	3.1	23.2	4.8

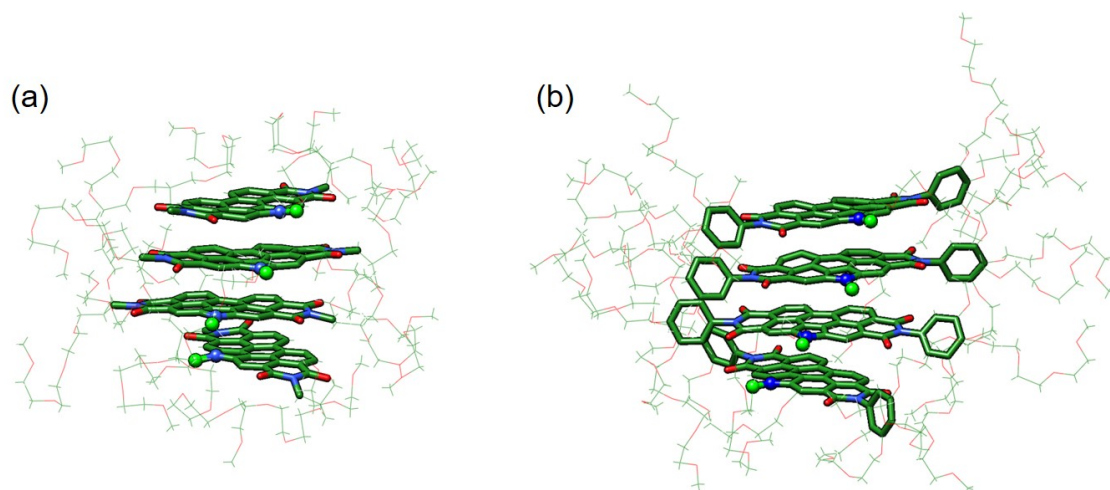


**Figure S10.** Detail of the helical-like supramolecular structure obtained for tetramers of *N*-PBIs **1** (a) and **3** (b) along the MD simulation. Some atoms are shown as spheres to highlight the helicity of the aggregate.

**Table S10.** Average values estimated for the electrostatic (Coulomb) and Lennard-Jones (LJ) energy terms along the MD trajectory of monomers and dimers of *N*-PBI **1** and **3**. The specific Coulomb interaction between the O atoms in the OEG chains and water is also shown for the same radius cutoff used during the dynamics and for a cutoff of 3.5 Å to isolate the contribution of hydrogen bonds. Finally, the average energy for a single hydrogen bond ( $E_{\text{H-bond}}$ ), obtained from the Coulomb (3.5 Å, OEG O) energy and the average number of hydrogen bonds given in Table S9, is also reported. All values are in kJ/mol.

<i>N</i> -PBI <b>1</b>	Coulomb	LJ	Coulomb (only H <sub>2</sub> O⋯O)	Coulomb (3.5 Å, OEG O)	$E_{\text{H-bond}}$
Monomer	-506.5	-187.1	-834.7	-55.1	-2.8
Dimer	-967.0	-325.9	-1586.3	-106.8	-2.9
<i>N</i> -PBI <b>3</b>	Coulomb	LJ	Coulomb (only H <sub>2</sub> O⋯O)	Coulomb (3.5 Å, OEG O)	$E_{\text{H-bond}}$
Monomer	-757.8	-299.7	-1235.3	-85.1	-3.1
Dimer	-1466.0	-501.8	-2382.3	-166.0	-3.3

## Calculations for related PBI and NBI systems

To extract more general structure-property relationships than those obtained for *N*-PBI **1** and **3**, we have also performed MD simulations for related PBI and NBI systems (PBI 1, NBI 3 and NBI 2 shown in Figure S11 and reported in Refs. 17a, 17b and 17c in the main text, respectively). Similar to *N*-PBIs **1** and **3**, our simulations are able to reproduce the experimental exothermic/endothemic character of the aggregation enthalpy for the related PBI and NBI systems; an endothermic aggregation enthalpy  $\Delta\bar{H}_{aggr}$  of 62 and 14 kJ/mol is predicted for those systems in which the extended OEG chains are attached to the core through a benzene bridge (PBI 1 and NBI 3, respectively). These findings are in line with the enthalpically disfavoured self-assembly process of *N*-PBI **3** reported in this study. Unlike PBI 1 and NBI 3, NBI 2, in which the trialkoxyphenyl moieties are connected to the NBI core via a methylene spacer, exhibits an enthalpically favoured self-assembly process with a  $\Delta\bar{H}_{aggr}$  value of  $-67$  kJ/mol. The origin at the molecular level of these different exothermic/endothemic enthalpy behaviour for the self-assembly of PBI 1, NBI 3 and NBI 2 is similar to that found for *N*-PBIs **1** and **3**; that is, the flexibility of the OEG side chains to reach the hydrophobic core and protect it from the solvent. Figure S12 displays the distance computed between the centroids of the  $\pi$ -core and the terminal segment of an OEG side chain (i.e., last  $-\text{OCH}_2\text{CH}_2\text{OCH}_3$ ) along the MD trajectory for all OEG side chains of PBI 1, NBI 3 and NBI 2. The comparison between PBI 1 (enthalpically disfavoured self-assembly) and NBI 2 (enthalpically favoured self-assembly) reveals that for PBI 1 only two side chains can effectively reach the central PBI core with close distances whereas all the side chains for NBI 2 can access to the NBI core with close and intermediate distances. This comes from the larger flexibility of the side chains in NBI 2 compared to PBI 1 due to the methylene spacer between the terminal trialkoxyphenyl units and the NBI core.

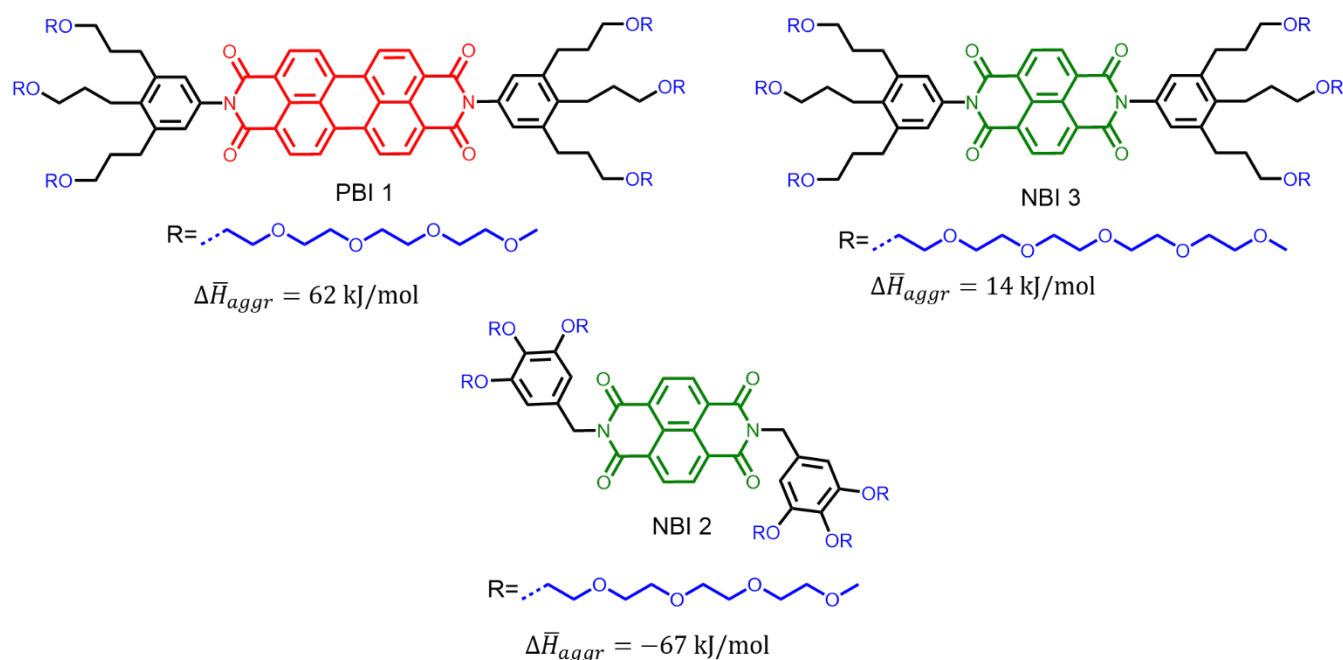


**Figure S11.** Chemical structures and aggregation enthalpies computed for related PBI and NBI systems (in particular, PBI 1, NBI 3 and NBI 2 from Refs 17a, 17b and 17c of the main text, respectively).

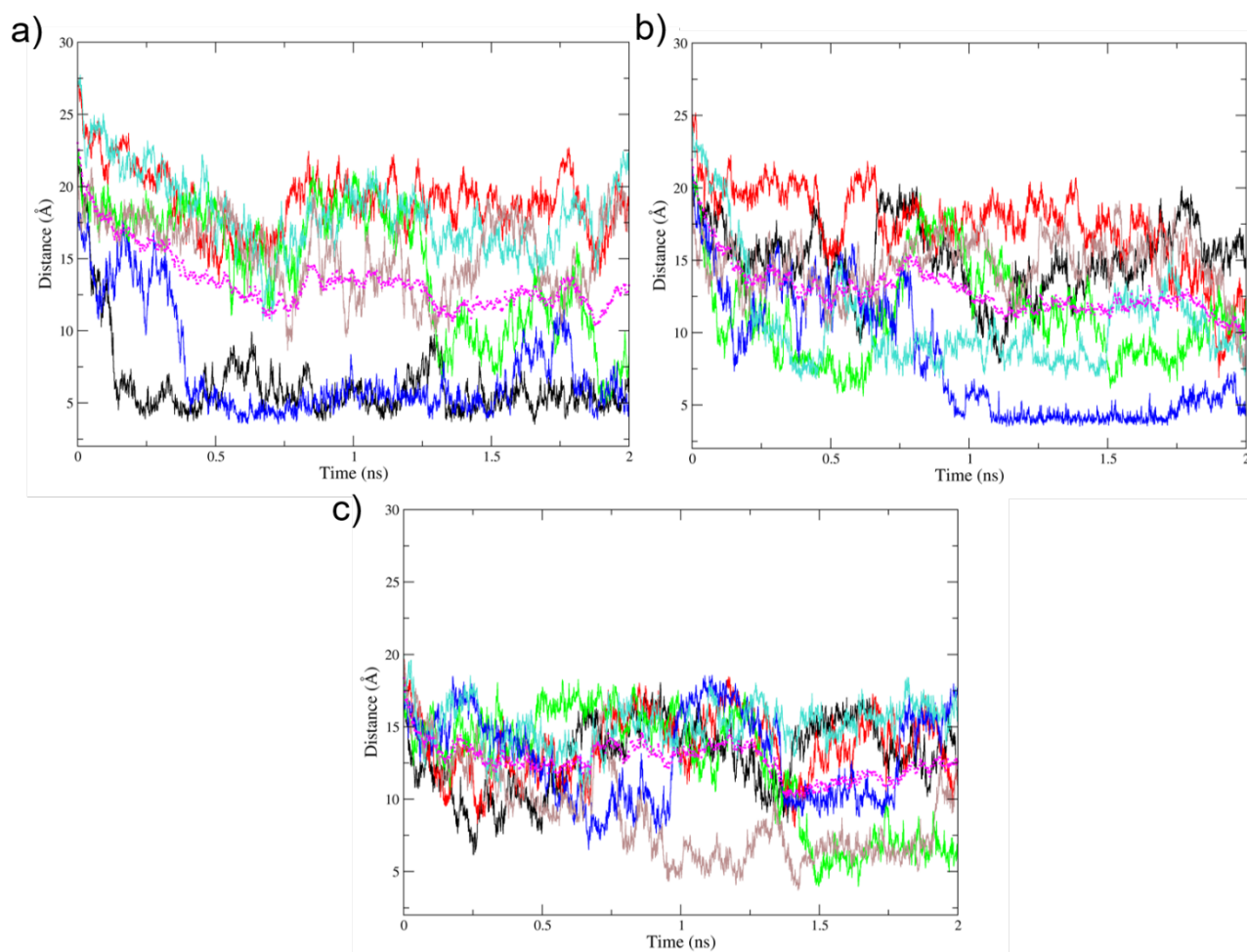


**Figure S12.** Distance between the centroids of the central  $\pi$ -core (PBI and NBI) and the terminal segment of an OEG side chain (i.e., last  $-\text{OCH}_2\text{CH}_2\text{OCH}_3$ ) along the MD trajectory for all OEG side chains (solid colours) of PBI 1 (a), NBI 3 (b) and NBI 2 (c) in water. The average value of this distance for all OEG side chains is represented in magenta.

## 5.- References

- S1 M. J. Abraham, T. Murtola, R. Schulz, S. Páll, J. C. Smith, B. Hess and E. Lindahl, *SoftwareX* **2015**, 1–2, 19.
- S2 M. Yabe, K. Mori and M. Takeda, *J. Comput. Chem. Jpn Int. Ed.* **2019**, 5, 2018.
- S3 C. Bannwarth, E. Sebastian and S. Grimme, *J. Chem. Theor. Comput.* **2019**, 15, 1652.
- S4 W. L. Jorgensen, J. Chandrasekhar, J. D. Madura, R. W. Impey and M. L. Klein, *J. Chem. Phys.* **1983**, 79, 926.
- S5 M. A. Martínez, E. E. Greciano, J. Cuéllar, J. M. Valpuesta and L. Sánchez, *Nanomaterials* **2021**, 11, 1457.
- S6 R. K. Gupta, D. D. S. Rao, S. K. Prasad and A. S. Achalkumar, *Chem. Eur. J.* **2018**, 24, 3566.
- S7 T. N. B. Truong, S. Savagatrup, I. Jeon and T. M. Swager, *Polym. Sci., Part A: Polym. Chem.* **2018**, 56, 1133.
- S8 S. Yamaguchi, A. Fukazawa and E. Yamaguchi, C. Wang WO2015111647 A1, **2015**.
- S9 J. Buendía, F. García, B. Yélamos and L. Sánchez, *Chem. Commun.* **2016**, 52, 8830.